

# Design of a Long Range Hydrogen Powered Transport

A project present to  
The Faculty of the Department of Aerospace Engineering  
San Jose State University

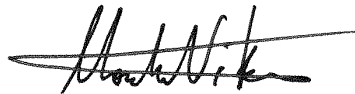
in partial fulfillment of the requirements for the degree  
*Master of Science in Aerospace Engineering*

By

**Matthew J. Smith**

May, 2016

approved by



Dr. Nikos Mourtos

Faculty Advisor



© 2016

Matthew J. Smith

ALL RIGHTS RESERVED

The Designated Project Advisor(s) Approves the Thesis Titled

DESIGN OF A LONG RANGE HYDROGEN POWERED TRANSPORT

by

Matthew J. Smith

APPROVED FOR THE DEPARTMENT OF AEROSPACE ENGINEERING

SAN JOSÉ STATE UNIVERSITY

May 2016

Dr. N. Mourtos

Department of Aerospace Engineering

Advisor

## ABSTRACT

### DESIGN OF A LONG RANGE HYDROGEN POWERED TRANSPORT

by Matthew J. Smith

Growing concerns over pollution and the rising costs of jet fuel has charged aviation companies to research into alternative fuels. Liquid hydrogen (LH<sub>2</sub>) is a promising alternative which is highly favorable due to its high specific energy content which makes it three times lighter than current jet fuels (Jet-A). In addition, LH<sub>2</sub>'s combustion with air produces water (H<sub>2</sub>O) and negligible amounts of harmful pollutants when compared with Jet-A. The major issue in adapting liquid hydrogen as a jet fuel would be its low energy density, requiring engineers to accommodate a fuel volume that is four times larger than Jet-A counterparts. In an effort to reduce the fuel volume, an unconventional blended wing body (BWB) configuration was selected for its large internal volume and high aerodynamic efficiency. Although BWB have several desirable qualities, there are significant drawbacks. BWB's have low maximum lift coefficients and difficulty in maintaining stability. Fortunately, BWB drawbacks can be mitigated to an extent when paired with LH<sub>2</sub> fuel. Although the high aerodynamic efficiency of a BWB configuration would significantly improve liquid hydrogen's chances at being a viable alternative jet fuel, its inherently heavier fuel system requirements would limit its usage to flights of over 7,000 nautical miles. As a result, the mission requirements and goals of the BWB-LH<sub>2</sub> design are similar to current high seating capacity long range conventional transport aircraft such as the B747 and A380. Conservative estimates on take-off weight and LH<sub>2</sub> fuel volume are 649,384 lbs and 203,575 US gallons, respectively. Through several iterations of the design, a reasonable balance between the fuel tanks and a 3-class passenger area is achieved. Although these two compartments are satisfied, there is a noticeable lack of luggage space. The overall concept of a BWB- LH<sub>2</sub> design is indeed feasible, although the current design presented in the report will need further optimization and testing before construction can begin. Current fuel prices for Jet-A1 and LH<sub>2</sub> will prevent concepts such as the BWB- LH<sub>2</sub> from entering production for at least two decades, but the switch to a cheaper and seemingly limitless fuel supply is inevitable.

## ACKNOWLEDGEMENTS

I would like to thank my advisor, Dr. Nikos Mourtos, for his guidance through the particularly difficult sections of this conceptual design. I would also like to thank the San Jose State University staff and students for their aid and support for the seven years I have spent on this campus. In particular, I would like to thank fellow students and graduates Brian Graham, Jimmy Rico, Matthew Miller, Arash Alex Mazhari, and Long Kim Lu for helping me through my many anxiety attacks. Last, I would like to thank my parents and older brother for their support and tutelage.

# TABLE OF CONTENTS

LIST OF TABLES .....	ix
LIST OF FIGURES .....	x
NOMENCLATURE .....	xi
1. PROLOGUE .....	1
1.1 Motivation .....	1
1.2 Background .....	3
1.2.1 Hydrogen.....	3
1.2.2 Blended Wing Body .....	4
1.3 Objective .....	7
1.3.1 Comparable Commercial Aircraft.....	7
2. MISSION .....	8
2.1 Mission Requirements .....	8
2.2 Mission Profile .....	8
3. MISSION WEIGHT ESTIMATION .....	9
3.1 Similar Aircraft and Hydrogen Adjustment .....	9
3.2 Mission Weight Determination .....	11
3.3 Weight Summary .....	14
4. PERFORMANCE SIZING .....	15
4.1 Equations and Example Calculations.....	15
4.1.1 Stall Velocity.....	15
4.1.2 Take-Off Performance .....	15
4.1.3 Landing Performance .....	16
4.1.4 Maneuvering Constraints .....	17
4.2 Matching Graph .....	18
4.3 Initial Drag Polar Calculations.....	19
5. CONFIGURATION SELECTION .....	20
5.1 Mission and Performance Goals .....	20
5.2 Propulsion Selection .....	21

5.3 Fuselage Selection.....	21
5.4 Empenage/Control Surface Selection.....	22
5.5 Configuration Model.....	22
6. INTERNAL VOLUME SETUP.....	23
6.1 Proposed Layout.....	23
6.2 Passenger Area.....	24
6.3 Hydrogen Fuel Storage.....	27
6.3.1 Hydrogen Fuel Tank Design.....	28
7. WING DESIGN.....	28
7.1 Centerbody Airfoil.....	28
7.2 Outboard Airfoil.....	30
7.3 Wing Analysis Program.....	32
7.4 Winglet Design.....	33
8. LANDING GEAR DESIGN.....	34
9. WEIGHT AND BALANCE.....	35
9.1 Fuselage/Centerbody Weight.....	35
9.2 Wing Weight.....	35
9.3 Engine Weight.....	36
9.4 Landing Gear Weight.....	36
9.5 Equipment and Subsystem Weight.....	37
9.6 Center of Gravity Calculations.....	39
10. STABILITY ANALYSIS.....	41
10.1 Longitudinal Stability.....	41
10.1.1 Coefficients.....	43
10.2 Lateral/Directional Stability.....	43
10.2.1 Differential Thrust Method.....	44
10.2.2 Split Aileron/Deceleron Method.....	45
11. DRAG POLAR.....	46
11.1 Drag Polar Plots.....	46
12. DISCUSSION.....	47
13. CONCLUSION.....	48

REFERENCES.....	49
APPENDIX A – Individual Fuel Tank Sizes.....	52
APPENDIX B – Airfoil Redesigns.....	55
APPENDIX C – Weight Sizing Matlab Code.....	56
APPENDIX D – Longitudinal Stability Matlab Code (Open Loop).....	58
APPENDIX E – Lateral/Directional Stability Matlab Code (Open Loop).....	61
APPENDIX F – Drag Polar Calculation and Plotting.....	64

## LIST OF TABLES

Table 1.1 Comparable aircraft specifications.....	7
Table 3.1 Similar aircraft characteristics (weight and range).....	9
Table 3.2 Short, medium, and long ranged hydrogen to kerosene weight ratios.....	9
Table 3.3 Hydrogen adjustment ratios and weights for similar aircraft.....	10
Table 3.4 Fuel weight fractions from Roskam and adjusted hydrogen values.....	12
Table 3.5 Fuel fraction and distance traveled breakdown by mission phase.....	13
Table 3.6 Microsoft Excel Solver function solution dump.....	14
Table 3.7 Weight summary of the aircraft.....	14
Table 5.1 Mission requirements related to design requirements.....	20
Table 6.1 Half-span chord lengths and section areas for BWB-LH2.....	24
Table 6.2 Cabin seating and width breakdown.....	26
Table 6.3 Fuel capacity per section breakdown.....	27
Table 7.1 Potential centerbody airfoils.....	29
Table 9.1 Weight sizing and center of gravity results.....	40
Table A.1 Section 1 fuel tank sizes.....	52
Table A.2 Section 2 fuel tank sizes.....	53
Table A.3 Section 3 fuel tank sizes.....	53
Table A.4 Section 4 fuel tank sizes.....	53
Table A.5 Section 5 fuel tank sizes.....	54
Table A.6 Section 6 fuel tank sizes.....	54

## LIST OF FIGURES

Figure 1.1 NASA+Boeing BWB versus 747 overlay.....	5
Figure 1.2 BWB seating configuration.....	5
Figure 1.3 Comparison of aerodynamic, inertial, and cabin pressure loads.....	6
Figure 2.1 Mission profile for arbitrary airplane.....	8
Figure 3.1 Weight ratios for take-off and empty aircraft for table 3.1 aircraft.....	10
Figure 3.2 Empty Weight vs Take-off weight of table 3.1 and table 3.3 aircraft.....	11
Figure 4.1 Matching graph for BWB-LH2 design.....	18
Figure 5.1 Initial volume division for fuel, luggage, and passenger compartments.....	22
Figure 5.2 Left-isometric view of BWB configuration (Open VSP 3.3.0).....	22
Figure 6.1 Top-down view of BWB section division.....	23
Figure 6.2 Example trapezoid to outline a, b, and h for equation 16 and figure 6.1.....	24
Figure 6.3 Cross section of BWB passenger/luggage compartments.....	25
Figure 7.1 MS-0317 Redesigned Airfoil Pressure distribution and $C_m$ vs $\alpha$ plot.....	30
Figure 7.2 MS-0317 Redesigned Airfoil $C_l$ vs $\alpha$ plot.....	30
Figure 7.3 NACA 0012 Supercritical Airfoil Outline.....	31
Figure 7.4 NACA 0012 Supercritical Airfoil $C_l$ vs $\alpha$ plot.....	31
Figure 7.5 NACA 0012 Supercritical Airfoil $C_m$ vs $\alpha$ plot.....	31
Figure 7.6 Wing Analysis Program experimentation.....	32
Figure 7.7 Winglet design illustration.....	33
Figure 8.1 Landing gear orientation.....	34
Figure 9.1 BWB-LH2 Weight-Center of Gravity Travel Diagram.....	41
Figure 10.1 Slatted Airfoil featuring a deceleron control surface.....	45
Figure 11.1 Drag Polar plot for ever configuration.....	46
Figure 11.2 Lift to drag plot for clean configuration.....	47
Figure B.1 TsAGIB-17% Airfoil retool design and $C_m$ vs $\alpha$ plot.....	55
Figure B.2 NACA 28117 Airfoil retool design and $C_m$ vs $\alpha$ plot.....	55

## NOMENCLATURE

A	State Matrix or Weight regression coefficient (Depending on section)
a,b	Chord base lengths (Trapezoid method)
A <sub>—</sub>	Area
a <sub>w</sub>	Lift curve slope
AC	Aerodynamic Center
AR	Aspect Ratio
atm	Atmosphere Unit of Pressure
B	Input Matrix or Weight regression coefficient (Depending on Section)
b	Wing Span
BWB	Blended Wing Body
C	Output Matrix
C <sub>D</sub>	Coefficient of Drag
C <sub>Dδ</sub>	Change in drag due to surface deflection
C <sub>j</sub>	Fuel Specific Consumption
C <sub>L</sub>	Coefficient of Lift
C <sub>Lδ</sub>	Change in lift due to surface deflection
C <sub>m</sub>	Coefficient of Moment
C <sub>m<sub>q</sub></sub>	Pitch Damping
C <sub>mα</sub>	Pitch Stiffness
C <sub>mδ</sub>	Control surface control power
C <sub>VT</sub>	Vertical Stabilizer Coefficient
C <sub>D0</sub>	Zero-Lift Drag Coefficient
CG	Center of Gravity
D	Drag or Feedthrough Matrix (Depending on section)
E	Endurance
e	Oswald's Efficiency

FAR	Federal Acquisition Regulation
ft	feet
H	Cylinder height
h	Distance between chords a and b
$I_{xx}, I_{yy}, I_{zz}, I_{xz}$	Moment of Inertia around axis
$K_n$	Static Margin
km	Kilometer
L	Lift
L/D	Lift to drag ratio
L <sub>allowed</sub>	Maximum length for cabin section
L <sub>VT</sub>	Distance between stabilizer and center of gravity
lbf	Pound Force
LH <sub>2</sub>	Liquid Hydrogen
M	Mach
n <sub>crosssectional rows</sub>	Number of rows in the seating compartment
nmi	Nautical Mile
p	Roll Rate
q	Pitch Rate
r	Cylinder radius
R	Range
r	Yaw Rate
$\rho$	Density of air
S	Wing Surface Area
S <sub>FL</sub>	Necessary Field Length
S <sub>L</sub>	Landing Distance
S <sub>TO</sub>	Take-Off Distance
S <sub>VT</sub>	Vertical Stabilizer Surface Area
T	Thrust
t/c	Airfoil thickness divided by chord length at wing root
TBA	To Be Announced

$u$	Axial Velocity
$V$	Velocity
$V_A$	Approach Velocity
$V_{\text{cylinder}}$	Cylinder volume
$V_S$	Stall Speed
$V_{SL}$	Landing Stall Velocity
$W$	Weight
$W_{\#}$	Weight fraction after each mission phase
$W_E$	Empty Weight
$W_{TO}$ or $TOGW$	Take-Off Gross Weight
$x_i$	Locaiton along x-axis
$X_{cg}$	Location along x-axis for center of gravity
$\alpha$	Angle of Attack
$\beta$	Side-Slip Angle
$\delta_a$	Aileron Deflection
$\delta_e$	Elevator deflection
$\delta_T$	Thrust Differential
$\delta$	Deceleron/Split Aileron Deflection
$\theta$	Pitch Angle
$\lambda$	Taper ratio
$\sigma$	Air stream density
$\phi$	Roll Angle

# 1. PROLOGUE

## 1.1 Motivation

Transportation plays an important role in the development of the world's economy. The desire for quick and efficient transportation over long distances prompted significant advancements in aviation. Post World War II, jet propelled commercial aircraft, such as the DH 106 Comet, became the preferred trans-Atlantic transportation method, trumping the propeller driven Bristol Type 167 Brabazon. While jet engines fulfill current transportation expectations, the fuel in which they operate have significant drawbacks.

The preferred commercial aviation fuel, Jet A (kerosene base), is comprised of hydrocarbon and sulfur molecules. The combination of kerosene with the nitrogen and oxygen molecules in air through combustion is given in equation 1.1. The “n”, “m”, and “x” subscripts are dependent on the formula of kerosene burned [1].

(1.1)

For every kilogram of kerosene and 3.4 kilograms of air there is roughly 3.15 kilograms of carbon dioxide (CO<sub>2</sub>), 1.25 kilograms of water (H<sub>2</sub>O), 14 grams of nitrogen oxides (NO<sub>x</sub>), 3.7 grams of carbon monoxide (CO), 1.3 grams of unburned hydrocarbons (HC), 1 gram of sulfur oxides (SO<sub>x</sub>), and 0.04 grams of black carbon (BC). Although the majority of these substances are low in quantity, their presence has a noticeable effect on the atmosphere [2]. Altering kerosene fuel blends and increasing engine efficiency will mitigate these emissions, but will never fully eliminate the environmental impacts. The availability of kerosene fuels is also a major concern for aviation companies. The most important component in kerosene is petroleum, a fossil fuel. Like other fossil fuels, petroleum supply is limited and depleting at a rapid rate. The depletion of petroleum causes kerosene prices to soar leading to a worrying increase in operating cost for kerosene powered aircraft [3]. To address these issues, aviation companies research alternative fuels such as liquid hydrogen (LH<sub>2</sub>). Hydrogen's specific energy is three times higher than kerosene. This means that the fuel weight for a liquid hydrogen aircraft is one third the fuel weight of its kerosene counterpart.

In addition to the specific energy advantage, hydrogen engines have little impact on the environment. The hydrogen and air molecules combine to produce water and trace amounts of nitrogen oxides. For every kilogram of hydrogen and roughly 8 kilograms of air, the combustion exhaust will consist of 9 kilograms of water and 4.3 grams of  $\text{NO}_x$ . Taking into consideration that a kilogram of hydrogen holds roughly the same energy as 3 kilograms of kerosene, the  $\text{NO}_x$  emission from hydrogen aircraft is roughly 10% of its kerosene counterpart. The formula for the combustion of hydrogen and air is given in the equation 1.2 [2].

(1.2)

In exchange for these benefits, hydrogen has a few properties that pose a challenge to aircraft designers. The leading challenge is dealing with hydrogen's relatively low energy density. Kerosene's energy density is four times greater than liquid hydrogen. This means that the fuel volume in a hydrogen aircraft is four times larger than its kerosene counterpart, despite being a third of the weight. Conventional aircraft configurations adapted for  $\text{LH}_2$  fuel require significant alterations to fuselage shape or reduction in passenger seating. This leads several hydrogen design concepts to employ unconventional configurations. The Blended wing body (BWB) configuration, with an inherently large internal volume and high aerodynamic efficiency, significantly improves hydrogen potential as an alternative jet fuel.

Although the BWB configuration alleviates several of  $\text{LH}_2$ 's drawbacks, new challenges arise as a result of the unconventional design. For example, BWB configurations have difficulty maintaining static stability without aft stabilizers and generally require sophisticated controllers for safe flight. In addition, BWB configurations also require careful balance between passenger, luggage, and aircraft subsystem compartments [4]. With modern engineering practices, BWB aircraft configurations are a viable alternative to conventional aircraft.

In today's market, Jet-A fuel is more economical as  $\text{LH}_2$  requires a significant amount of resources to manufacture and explaining why aviation companies continue to favor kerosene over other alternative fuels [3]. Current cost analysis models predict that Jet A and  $\text{LH}_2$  prices will equate by the year 2040 [5]. The aviation industry's switch to liquid hydrogen would ensure

lower green house gas emissions and access to a near limitless supply of fuel, explained in section 1.2.1

## **1.2 Background**

### **1.2.1 Hydrogen**

It should be noted that hydrogen should not be considered an energy “source”, but rather an energy “carrier”. In other words, hydrogen acts more like a single use battery than fuel. Unlike fossil fuels, hydrogen requires a significant amount of energy to produce. The collection of pure hydrogen is the result of expending energy to separate hydrogen from hydrogen carrying molecules. That is to say, the supply of hydrogen is related to the supply of hydrogen carrying molecules, such as water. Therefore the supply of hydrogen is seemingly limitless. There are two methods for acquiring hydrogen: reforming natural gas and electrolysis [2]. Reforming natural gas produces 90% of all hydrogen fuels, but it is also the method which produces the most green house gas emissions. In this method, natural gasses are broken down into hydrogen and carbon dioxide which gives way to criticism that hydrogen fuel production may provide as much or more pollution than current fossil fuel vehicles. The second method, electrolysis, breaks down water molecules, producing hydrogen and oxygen molecules. This method, although relatively new, is the preferred hydrogen manufacturing process as it produces no green house gas emissions and only uses water and electricity for reactants [2, 3]. Future expansion of green energy methods for producing electricity would ensure that LH<sub>2</sub> would be the most environmentally friendly fuel option [3].

Hydrogen fuels have two states: gas and liquid. While both hydrogen states have the same specific energy, their energy densities are different. The energy density of liquid is much higher and thus more suitable for use in aviation. However, LH<sub>2</sub> is extremely volatile and must be well insulated and pressurized to prevent the fuel from prematurely boiling-off and permeating through the walls. Hydrogen requires a temperature of at least -253<sup>o</sup> Celsius to maintain liquid form at 1 atm, although this temperature value does increase through pressurization of the tanks. Installation aboard an aircraft would require that the fuel tanks be insulated with cryogenic foam and constructed with sufficiently thick walls [3]. Hydrogen storage containers are ideally spherical in shape to maintain such environmental demands. From

an engineering standpoint, the use of cylindrical fuel tanks should prove adequate and allow for installation inside of wing structures [2, 3].

The idea of switching aircraft from Jet A to LH<sub>2</sub> may seem like a revolutionary advancement, but it's not actually new to aviation. In 1937, the first German jet engine prototype, Heinkel HeS-1, was powered completely by hydrogen [6]. In 1956, NACA modified a B-57 to fly completely on LH<sub>2</sub> through the use of a heat exchanger to change the LH<sub>2</sub> into a gas that will flow into the combustor. Two LH<sub>2</sub> tanks mounted on the wings were able to power the B-57 for a little over 20 minutes before landing [5]. The Russians also experimented with liquid hydrogen in the event that their own fuel supplies were difficult to obtain. Russian aircraft manufacturer, Tupolev, modified a Tu-154 to test the capabilities of liquid hydrogen as an alternative fuel. In April of 1988, the modified Tu-154 (renamed to the Tu-155), successfully proved that liquid hydrogen is a viable alternative fuel source for their commercial aircraft [5].

In recent years, interest in fuel cell technology re-invigorated hydrogen fuel research. Although fuel cells can only power electric motors, they boast a higher efficiency than internal combustion engines, further reducing the fuel volume required for flight. NASA published a concept for an aircraft powered by eight ducted fans using hydrogen fuel cells. The goal of the design was to reduce green house gas and noise pollution with comparable performance goals of a conventional transport [7]. Although thrust levels for this aircraft were fairly low, the actual results indicated that this aircraft would be well suited for short distance flights.

A fundamental flaw in the LH<sub>2</sub> aircraft design is the inclusion of well insulated fuel tanks that not only require a great deal of internal volume, but also increase the overall empty weight of the aircraft. For short and medium range jet aircraft, the conversion to hydrogen fuel will result in a lower efficiency (18% and 5% lower respectively) than their Jet-A counterparts. However, long range missions of over 7,000 nautical miles will result in a fuel efficiency increase of 12% [8].

### **1.2.2 Blended Wing Body**

It should come to no surprise that the hydrogen fuel cell and ducted fan concept in section 1.2.1 utilizes a BWB design to improve their aircraft's performance [7]. Similar to hydrogen powered aircraft, blended wing body configurations are not a new concept. In the 1920's,

William Bushnell Stout designed the Batwing aircraft as a method for reducing an aircraft's drag [9]. Commercial aviation also experimented with blended wing body designs. The Junkers G38 transport plane, although designed with an empennage, utilized a thick wing root which allowed for engineers to comfortably observe and maintain the engines during flight [9]. In recent years, NASA and Boeing have published numerous commercial BWB aircraft concepts. One such conceptual design was intended to outperform current large scale commercial transport aircraft. Its size would be comparable to a Boeing 747, but could carry almost twice the number of passengers. This also translates into lower fuel cost per passenger than standard tube fuselage aircraft [10]. Figure 1 illustrates the size differences between the two aircraft.

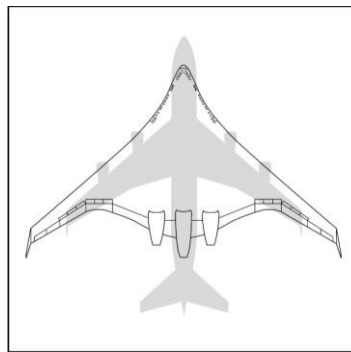


**Figure 1.1: NASA+Boeing BWB versus 747 overlay [11].**

While there are significant advantages in passenger accommodation, it should be noted that BWB cabins are more difficult to pressurize and have unfavorable seating arrangements in comparison to standard tube fuselages. Initial BWB fuselage passenger seats were oriented much like a theatre, which may be considered as uncomfortable for the passengers. To pressurize and reduce the number of seats per row, designers suggest separating the internal space into multiple tube cabins. Figure 1.2 illustrates the separated compartments [11].

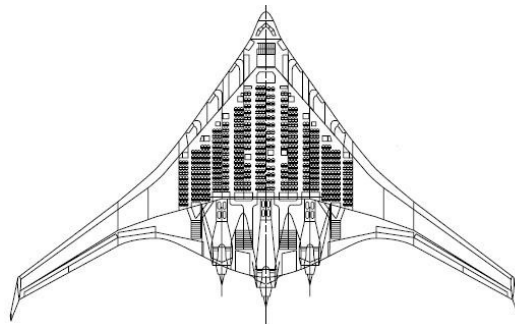


**Figure 1.2: BWB seating configuration [11]**

The aerodynamic efficiency of BWB designs stem from one main characteristic: high lift to drag ratios in cruise. The BWB design minimizes wetted area, reducing skin friction drag by as much as 33% in comparison to conventional designs [12]. Although the skin friction drag is reduced, the thick centerbody shape is susceptible to flow separation. Several simulations and iterations of the aircraft's centerbody airfoil will need to be conducted to optimize airflow over the surface [11]. The spanwise lift inherent in BWB configurations utilizes the airfoil shaped centerbody fuselage to complete the elliptical lift distribution. Proper spanwise lift distribution and smooth interconnection between the wing and fuselage can significantly improve aerodynamic efficiency [10]. Consequently, this spanwise lift distribution will require special manufacturing using advanced composite materials to circumvent fatigue as a result of additional inertial loads on the fuselage and wing root sections [12]. The lift, inertial load, and cabin pressure distribution for conventional and BWB configurations are illustrated in figure 1.3.

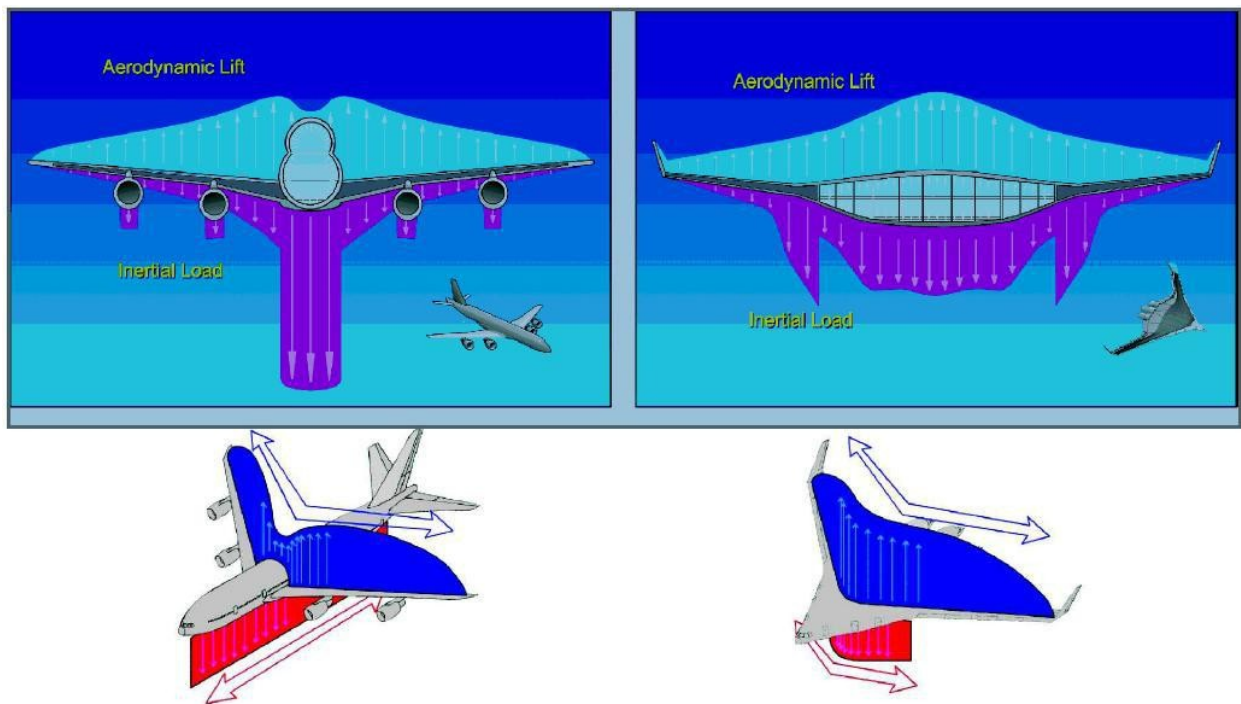


Figure 1.3: Comparison of aerodynamic, inertial, and cabin pressure loads [12]

### 1.3 Objective

The objective of this project is to design a long range, liquid hydrogen powered, blended wing body aircraft for commercial transport. The intent is to provide an alternative to conventional configuration Jet-A fueled aircraft. The seating capacity goal is a minimum of 550 passengers with a range of at least 7,500 nautical miles (nmi).

#### 1.3.1 Comparable Aircraft

A comparison of future and current commercial aircraft is presented in table 1.1. It should be noted that despite the high seating capacity of blended wing body designs, the maximum gross weight is closer in magnitude to the A340-600 than the A380-800. The maximum seating capacity for the A380 is stated as 853 passengers, but typical passenger size is 544 for a 4-class accommodation [15].

Table 1.1: Comparable aircraft specifications [11, 13, 14, 15, 16, 17]

<b>Comparable Aircraft</b>					
<b>Aircraft</b>	<b>Seating Capacity</b>	<b>Range (nmi)</b>	<b>Maximum Thrust (lbf)</b>	<b>Maximum Gross Weight (lbs)</b>	<b>Maximum Fuel Capacity (US gallons)</b>
Boeing 747-8	515	7,700	266,000	990,000	63,034
Boeing 777-9	425	8,700	204,000	TBA	TBA
Airbus 380-800	853	8,200	280,000	1,268,000	84,600
Airbus 340-600	475	7,800	240,000	811,300	51,750
NASA+Boeing BWB	800	7,000	TBA	823,000	TBA

## 2. MISSION

### 2.1 Mission Requirements

The mission for this hydrogen powered, blended wing body aircraft is similar to other commercial aircraft. Many of the mission requirements are similar to current commercial airliners.

- Payload
  - o 550 passengers and associated luggage
  - o 15 crew members
  - o Liquid Hydrogen fuel and associated insulated tanks
- Cruise
  - o Altitude of 35,000 ft
  - o  $M=0.85$
- Range
  - o 7500 nautical miles (nmi)
  - o Additional fuel for 1 hour of loiter and 5% extra fuel supply
- FAR-25 Certification (Federal Acquisition Regulation)
  - o Take-Off distance: 9,000ft
  - o Landing distance: 6,300ft

### 2.2 Mission Profile

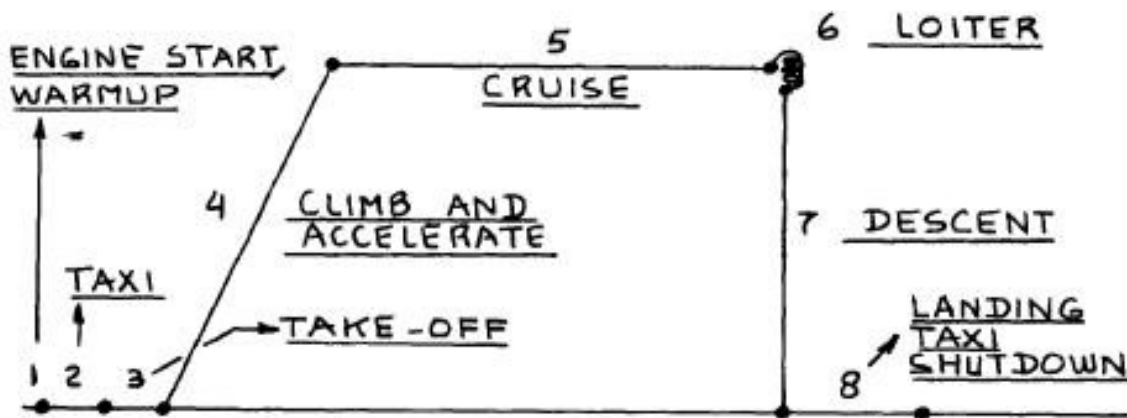


Figure 2.1: Mission profile for arbitrary airplane[18].

### 3. MISSION WEIGHT ESTIMATION

#### 3.1 Similar Aircraft and Hydrogen Adjustment

Through the years there have been a handful of successful flying wing and BWB designs which one can formulate a set of regression coefficients from. Table 3.1 lists a few similar aircraft along with their take-off weight ( $W_{TO}$ ), empty weight ( $W_E$ ) and range.

**Table 3.1: Similar aircraft characteristics (weight and range) [11, 19, 20, 21]**

Aircraft	$W_{TO}$	$W_E$	Range	
	(lbs)	(lbs)	(nmi)	
XB-35	209000	120000	13100	7073
YB-49	193938	88442	16057	8670
B-2	376000	158000	11112	6000
BWB-450	823000	412000	12964	7000

However, LH<sub>2</sub> powered aircraft are still in their infancy stages. The combination of BWB designs for LH<sub>2</sub> aircraft has either only been conceptualized or is classified by aviation manufacturers. Using Verstraete's analysis from reference 8 as a guide, it is possible to adjust the kerosene aircraft to a hydrogen fuel source, at least as far as weight is concerned. The weight ratios and aircraft ranges from reference 8 are given in table 3.2.

**Table 2.2: Short, medium, and long ranged hydrogen to kerosene weight ratios [8].**

	Range		$W_{TO}$	$W_E$
	km	nmi	ratio to kerosene aircraft	
Short	4000.00	2159.83	1.11	1.36
Medium	9000.00	4859.61	0.94	1.28
Long	14000.00	7559.40	0.71	1.03

The weight ratio adjustments were calculated as a function of range as hydrogen's take-off weight advantage is dependent on its mission range. Table 3.3 lists the ratios and adjusted weights for each aircraft in table 3.1.

Table 3.3: Hydrogen adjustment ratios and weights for similar aircraft.

Aircraft	Range (nmi)	W <sub>TO</sub> ratio	W <sub>E</sub> ratio	W <sub>TO</sub> Adjusted (lbs)	W <sub>E</sub> Adjusted (lbs)
XB-35	7073.43	0.76	1.09	158081.37	130354.58
YB-49	8670.09	0.60	0.87	117237.00	76918.92
B-2	6000.00	0.85	1.20	319087.59	189078.63
BWB-450	7000.00	0.76	1.09	627894.76	451034.20

Figure 3.1 illustrates the weight ratios and gives the 2<sup>nd</sup> order polynomial trend line equations used to calculate the weight ratios listed in table 3.3. The black squares are the weight ratios for aircraft from table 3.1. Figure 3.2 compares the hydrogen adjusted aircraft with their kerosene counterparts in an empty weight versus take-off weight plot.

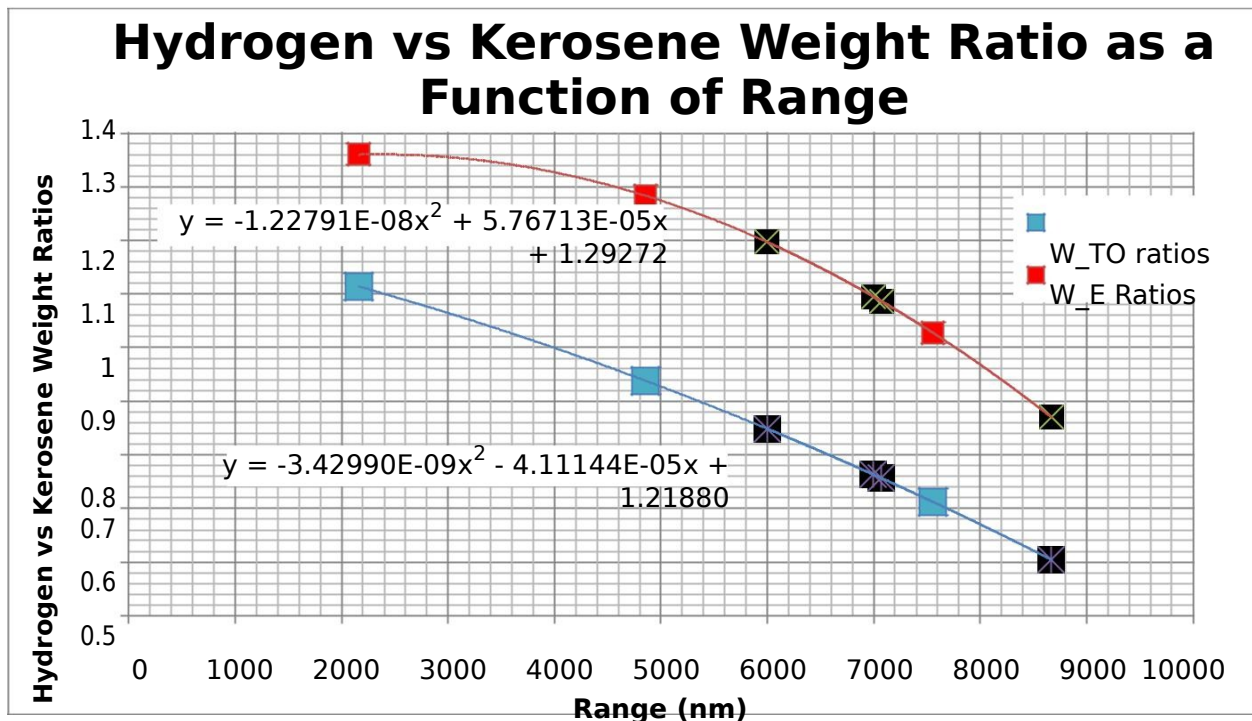


Figure 3.1: Weight ratios for take-off and empty aircraft. Black boxes indicate table 3.1 aircraft specific weight ratios

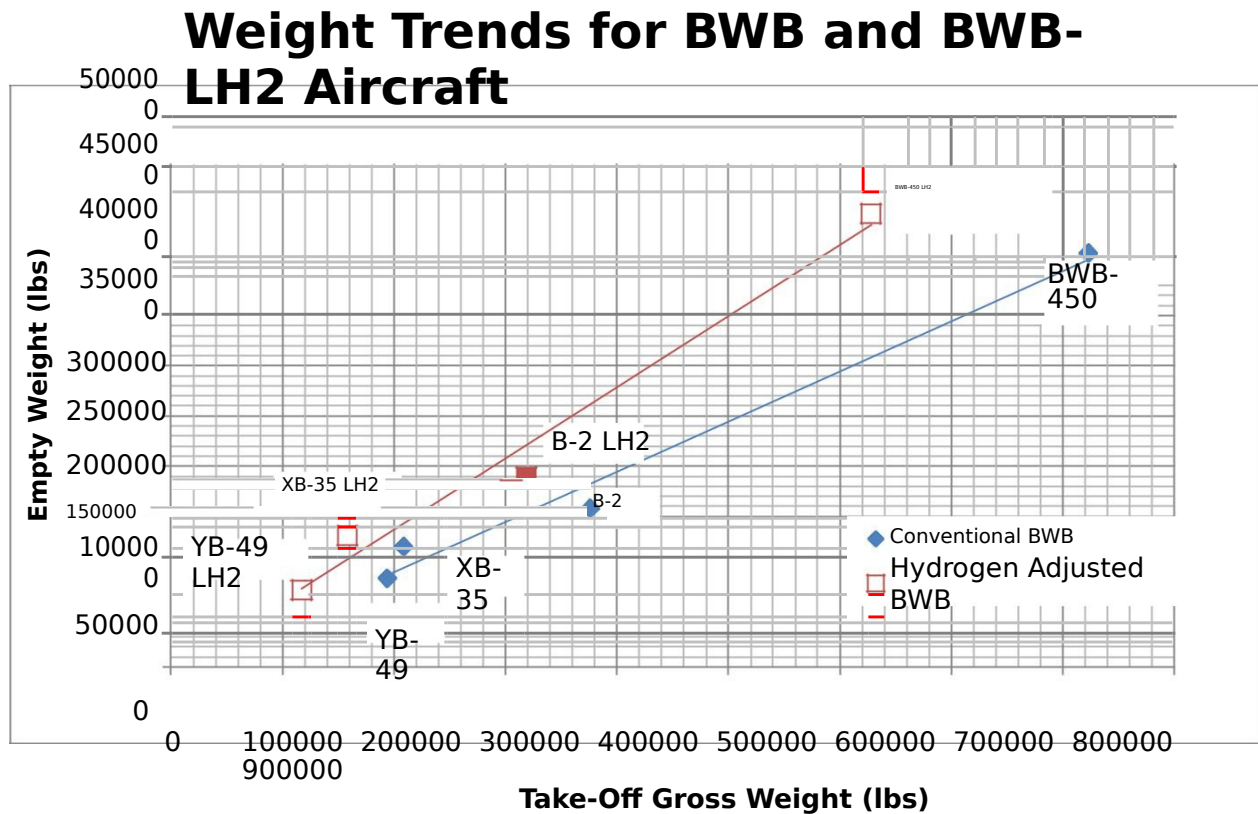


Figure 3.2: Empty weight versus take-off weight of table 3.1 and table 3.3 aircraft.

### 3.2 Mission Weight Determination

Mission weight estimates can be calculated using a method outlined in the first part of Roskam's *Airplane Design* [18]. Several of the coefficients have been changed to account for the differences in aircraft weight as a result of each phase outlined in the mission profile. To initiate the process, an initial guess to take-off weight ( $W_{TO}$ ) is made and refined until the difference between empty weights ( $W_E$ ) calculated through fuel burn and calculated through regression coefficients are virtually zero. This optimization process is handled in Microsoft Excel Spreadsheet using the Solver function to minimize this difference by varying the take-off weight guess.

In the previous section, a hydrogen adjustment was performed on a BWB-450 aircraft. This aircraft is capable of take-off with around 800 passengers and a 7000 nautical mile range [11]. This aircraft should provide a suitable initial a take-off guess as its dimensions would be similar to the conceptual BWB- LH<sub>2</sub> design. Payload weight is calculated using Roskam's method which assumes a passenger weight of 175 lbs and luggage weight of 40 lbs while each crew member weighs 175 lbs and carries 30 lbs of luggage [18]. Mission fuel weight is found using a fuel fraction method. These fuel fractions were formulated using kerosene based fuel and



thus unsuitable for hydrogen. These ratios can be adjusted by reducing the weight loss to a third of what was previously lost. The adjusted values are given in table 3.4 along with the original values given by Roskam [18].

**Table 3.4: Fuel weight fractions for Roskam and adjusted hydrogen values [18].**

	<b>Engine Startup</b>	<b>Taxi</b>	<b>Take-Off</b>	<b>Climb</b>	<b>Descent</b>	<b>Landing</b>
Roskam's Values	0.99	0.995	0.995	0.99	0.99	0.992
Hydrogen Adjusted	0.9967	0.9967	0.9983	0.9667	0.9967	0.9973

Cruise and loiter fuel fractions were calculated using equations 3.1 and 3.2. Equation 3.1 uses the range (R) formula to calculate cruise fuel fraction ( $W_5/W_4$ ) and equation 3.2 uses the endurance (E) formula to calculate for loiter fuel fraction ( $W_6/W_5$ ).

$$\frac{W_5}{W_4} = \frac{W_4}{W_4} \left( \frac{R}{R_0} \right)^{\frac{1}{L/D}} \quad (3.1)$$

$$\frac{W_6}{W_5} = \frac{W_5}{W_5} \left( \frac{E}{E_0} \right)^{\frac{1}{L/D}} \quad (3.2)$$

Velocity ( $v$ ) at cruise is 490kts. The assumed lift-to-drag (L/D) values are expected from previous BWB configurations: 21 for cruise and 24 for loiter [19]. Fuel specific consumption ( $C_j$ ) for hydrogen is less than half of values published for kerosene. The  $C_j$  values of 0.2 for cruise and 0.15 for loiter are fairly conservative values when taking into consideration the differences in specific energies between hydrogen and kerosene. A final breakdown of these fuel fractions and the overall mission fuel fraction is calculated using equation 3.3. Table 3.5 shows overall fuel fraction breakdown and distances of each phase.

$$\frac{W_{total}}{W_{total}} = \frac{W_{total}}{W_{total}} \left( \frac{W_5}{W_4} \right) \left( \frac{W_6}{W_5} \right) \dots \quad (3.3)$$

**Table 3.5: Fuel fraction and distance traveled breakdown by mission phase.**

<b>Phase</b>	<b>Variable</b>	<b>Value</b>	<b>Distance</b>
Engine Start-Up/Warm-up	$W_1/W_{TO}$	0.9967	0
Taxi	$W_2/W_1$	0.9967	0
Take-Off	$W_3/W_2$	0.9983	0
Climb	$W_4/W_3$	0.9667	83.33
Cruise	$W_5/W_4$	0.8670	7416.67
Loiter	$W_6/W_5$	0.9969	0
Descent	$W_7/W_6$	0.9967	0
Landing/Taxi/Shutdown	$W_8/W_7$	0.9973	0
Start-up to shutdown	$W_8/W_{TO}$	0.823593	7500

The empty weight can then be calculated by deducting the payload, crew, and total fuel from the take-off weight guess. This empty weight is compared to the empty weight calculated using equation 3.4. This equation uses A and B as assumed regression coefficients from previous aircraft data where  $A=0.0665$  and  $B=1.0248$ .

---

(3.4)

The spreadsheet optimized solution is given in table 3.6 in which the difference between the two calculations is zero. The take-off weight is roughly 79% the weight of the BWB-450, which is to be expected of an aircraft which has made a transition to hydrogen fuel. The weight can even be lower, but conservative values for fuel specific consumption were used.

**Table 3.6: Microsoft Excel Solver Function solution dump.**

<b>Weight Calculation</b>	<b>Value</b>	<b>Unit</b>
$W_{TOguess}$	649383.77	lbs
$W_{Fuel\ Used}$	114555.6	lbs
$W_{OEtentative}$	410850.4	lbs
$W_{Etentative}$	404528.5	lbs
Allowable $W_E$	404528.5	lbs

From this final iteration, calculations for the total volume needed for storing fuel are completed. Taking the weight of the fuel used and adding in 5%, the final volume requirement for integrating in LH<sub>2</sub> is 203,575 US gallons. This value is within reasonable bounds as the energy density of hydrogen is four times that of kerosene. Comparable aircraft such as the B747 use around 62,000 US gallons of Jet-A, leading to an expected 248,000 US gallons if it were to convert to LH<sub>2</sub> fuel supply [13]. The change to a blended wing body design saves more fuel and provides more internal volume in comparison to conventional, allowing for LH<sub>2</sub> to be a viable alternative to Jet-A in commercial flights.

### 3.3 Weight Summary

**Table 3.7: Weight summary of all weight components of the aircraft.**

Crew Weight (15 crewmen)	3,075	lbs
Passenger (Payload) Weight (550 passengers)	118,250	lbs
Total Fuel Weight (used +reserve)	120,284	lbs
Empty weight	404,529	lbs
Trapped Fuel and Oil Weight (0.5%)	3,246	lbs
Estimated Take-Off Weight	649,384	lbs

## 4. PERFORMANCE SIZING

### 4.1 Equations and Example Calculations (FAR 25)

All equations use Roskam's preliminary sizing method from reference 18.

#### 4.1.1 Stall Speed

Equation for stall speed and isolation of wing loading:

$$V_{stall} = \sqrt{\frac{W}{S C_{Lmax} \rho}} \quad (4.1)$$

Example: Take a usual stall speed of around 125kts (211ft/s) or 150kts (253ft/s) without high lift devices. The BWB is at an elevation of 5,000 feet where the air density is 0.00197slugs/ft<sup>3</sup>. Normally the maximum coefficient of lift for BWB is low (around 1.2) as a result of flapless wings. However, including slats to the wing may increase the coefficient of lift to around 1.5. Calculating with high lift devices and without (clean):

$$\frac{W}{S} = \frac{1}{2} \rho V_{stall}^2 C_{Lmax}$$

#### 4.1.2 Take-Off Performance

Equation for take-off distance and isolation of thrust to weight ratio:

$$SOD = \frac{1.8 W^{0.5}}{g C_{Lmax} \rho^{0.5}} \quad (4.2)$$

Example: Comparable aircraft have take-off distances around 9000ft. Keeping the same altitude of 5,000 feet (pressure ratio  $\delta=0.8320$ ) and experiencing a change in temperature of 20°

Fahrenheit from 80° Fahrenheit ( $\theta=1.0385$ ). Assume at coefficient of lift maximum of 1.5.  
 Assume a wing loading of 50 lb/ft<sup>2</sup>. Air steam density  $\sigma=\delta/\theta=0.832/1.0385=0.8$

$$\frac{W}{S} = \frac{1}{2} \rho V^2 C_L$$

### 4.1.3 Landing Performance

Equation for landing wing loading:

$$\frac{W}{S} = \frac{1}{2} \rho V^2 C_L$$

(4.3)

Equations for landing stall speed and approach speed in kts\*:

$$V_{stall} = \sqrt{\frac{2W}{\rho C_L}}$$

(4.4)

$$V_{approach} = 1.3 V_{stall}$$

(4.5)

Equation for necessary field length:

$$L = \frac{V_{approach}^2}{g}$$

(4.6)

Example: Landing at a field at an elevation of 5,000ft, with a coefficient of lift of 1.3, and landing distance of 6,000ft.

$$L = \frac{V_{approach}^2}{g}$$

$$=$$

$$= \frac{(1.3 \sqrt{\frac{2W}{\rho C_L}})^2}{g}$$

#### 4.1.4 Maneuvering Performance

Equation for thrust to weight ratio when maneuvering with load factor, n:

$$\frac{T}{W} = \frac{n}{\eta}$$

(4.7)

Example: Assume load factor 2, wing loading  $50 \text{ lb/ft}^2$ , aspect ratio 6, and Oswald efficiency 0.85. For climb the speed is generally 250kts or 422ft/s at an altitude of 5,000 ft. This means dynamic pressure q is 175.4slug/(ft-s). The zero lift drag coefficient on this BWB is 0.0075.

$$\frac{T}{W} = \frac{n}{\eta} = \frac{2}{0.85} = 2.35$$

## 4.2 Matching Graph

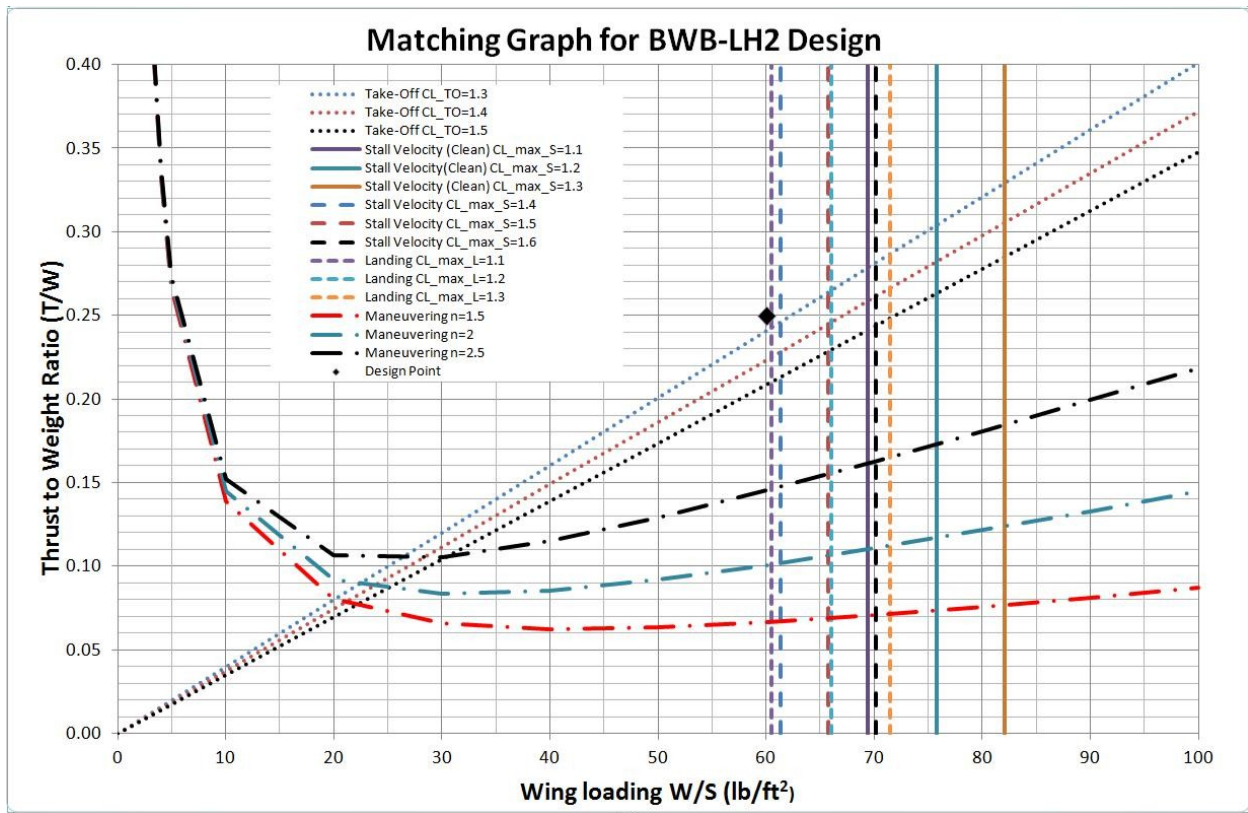


Figure 4.1: Matching Graph for BWB Design

From the matching graph, an initial design point was chosen to be at a wing loading of 60 lb/ft<sup>2</sup> and thrust to weight ratio of 0.25. This point was selected because it uses a reasonable expectation of what the aircraft's coefficient of lift will be for take-off conditions. From the graph, it is easy to see how challenging it is to create a BWB and flying wing aircraft as their coefficient of lift is restricted without using high lift devices. To achieve a lift to drag ratio expected of BWB designs, compromises with certain components need to be made. The thrust to weight ratio is relatively average for flying wing and BWB designs. With the current weight estimates from section 2, the minimum wing area is 10,823ft<sup>2</sup> and the minimum thrust required is 162,323.6 lbf. The maximum coefficient of lift at take-off is 1.3 and coefficient of lift for landing is 1.1. The aspect ratio for the aircraft, as used in the maneuvering calculations, is 6.5. The wingspan is calculated to be 245ft.

### 4.3 Initial Drag Calculations

Producing initial drag calculations is helpful for determining if the assumed L/D values are viable. Using Raymer's method, the zero lift drag coefficient,  $C_{D0}$ , is calculated using equation 4.8. [22].

---

(4.8)

Here  $C_{fe}$  is the equivalent skin friction coefficient and it is generally estimated to be around 0.003. Flying wings and blended wing bodies tend to have a wetted to reference area of 2.5, so the estimated zero lift drag coefficient is 0.0075, which is referenced in section 3.1.4 of this report [22]. Roskam and Raymer provide roughly the same values for change in zero lift drag coefficient and Oswald efficiency. These changes affect the overall drag coefficient formula given in equation 4.9 [18, 22].

---

(4.9)

The changes in coefficient of drag are related to current flap and landing gear phases. While flaps or flaperons, deflected minimally, may improve landing performance without greatly impacting the pitching moment, their presence may not be needed for this current stage of design as the take-off and landing performance estimations are well within allowable limits. The coefficient of drag at each phase of take-off and landing procedures are given below. Gear position and phase of flight have an impact on the change in zero-lift drag [18, 22]. These formulas are all with clean configuration, meaning no high lift devices.

Low speed flight with gear up, clean configuration:

Take-off with gear down, clean configuration:

Take-off with gear up, clean configuration:

Landing with gear up, clean configuration:

Landing with gear down, clean configuration:

## 5. CONFIGURATION SELECTION

### 5.1 Mission and Performance Goals

Table 5.1: Mission requirements related to design requirements

<b>Mission Requirements/Performance Goals</b>	<b>Design Requirements</b>
Liquid Hydrogen Fueled Propulsion System	Large internal volume, efficient cooling system and fuel tank insulation
Comfortable flight for passengers	Fewer seats per section, seats located close to the roll axis, interactive displays to replace window seats.
Pressurization of fuselage	Divide the interior section into compartments
Absence of conventional horizontal stabilizers	Specialized wing and centerbody airfoil selection
Absence of conventional vertical stabilizers	Installation of large winglets/split ailerons/differential thrust to maintain directional control
Achieving high L/D ratios	High wing loading, reduction of components that cause drag

## **5.2 Propulsion Selection**

Designing a propulsion system around the required thrust of 162,325 lbf shouldn't be too difficult. Dividing the requirement among three turbofan engines would simply require each engine to output 54,110 lbf. The 747-8's turbofan engines have an upper limit of 70,000 lbf [23]. The current requirements for a three turbofan propulsion system can be safely satisfied by engines lesser than what is installed on the 747-8.

Installing turboprop engines with a fuel cell powered electric motor is a viable alternative to internal combustion engines in the current plan. The efficiency would be significantly improved, leading to far less fuel storage. However, the current market of long distance commercial airliners requires a relatively short flight time. Extending the flight time in exchange for higher fuel efficiency isn't a desirable trade-off for potential passengers.

## **5.3 Fuselage Selection**

Before the internal volume of the cabins can be situated, it is important to select a general body shape. Hybrid BWB designs take advantage of the inherent lifting body design while maintaining a comfortable inner space. However, these hybrid BWB designs lack a great deal of internal volume needed for liquid hydrogen storage. A smooth transition from outboard wing to centerbody would provide a substantial increase to the aircraft's internal volume.

The internal compartments should be designed in such a way that the individual compartments can be pressurized and the number of seats per row limited to 5-6 across the aisle. The initial blueprint utilizes the planned BWB-450 layout while removing the outer passenger compartments to free up room for fuel storage. The current plan of separating the passenger volume into six compartments allows for ease of cabin pressurization and divides the theatre-like passenger seating for passenger comfort. A major drawback may be with luggage accommodation. Overhead compartments may need to have increase in space to accommodate larger bags. An illustration taken from George M. Buch Jr.'s research paper has been altered to visualize the internal compartment configuration [24]. The illustration is given in figure 5.1.

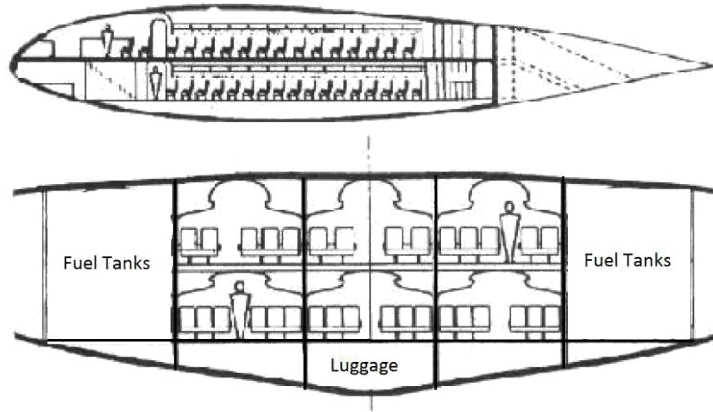


Figure 5.1: Initial volume division for fuel, luggage, and passenger compartments [24].

#### 5.4 Empennage/Control Surface Selection

The current selection for directional control is the installation of large winglets and split ailerons or decelerons near the wingtip. Vertical stabilizers on either side of the three engines was considered as a viable solution to maintaining lateral control, however, winglets and lateral control mechanisms were shown to perform similar tasks while improving the aerodynamic performance of the BWB. Through the installation of winglets, it is possible to inhibit the formation of wingtip vortices and lower induced drag. For yaw control, the use of differential drag surfaces near the wingtip will be utilized. In the event these drag surfaces provide insufficient yaw control, the use of differential thrust may be included into the BWB systems.

#### 5.5 Configuration Sketch

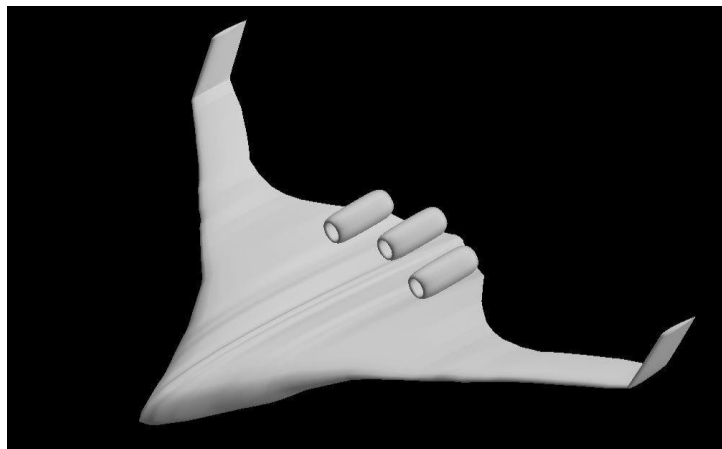


Figure 5.2: Left-Isometric View of BWB configuration created in OpenVSP 3.3.0

## 6. INTERNAL VOLUME LAYOUT

### 6.1 Proposed Setup

Balancing the unusual blended wing body shape is a delicate process. With a hydrogen aircraft the internal area of the aircraft is greatly reduced to accommodate the excessive fuel storage, further complicating the process. Adjusting the external shape of the BWB turned into an iterative process until the passenger area and hydrogen fuel storage achieved a sufficient amount of space. Designing the shape of the BWB started with a baseline top-down outline of the aircraft given in figure 6.1. The outline was halved and split into eight trapezoidal sections. The equation for a trapezoid's area is given in equation 16. Each trapezoidal section lengths and areas are given in table 6.1. Figure 6.2 labels the locations of “a”, “b”, and “h” for reference. It should be noted that the blue highlighted section 4 is the location where the outboard airfoil transforms into the centerbody airfoil. The overall wing area is 3.8% greater than what is required from the matching graph which is well within acceptable limits.

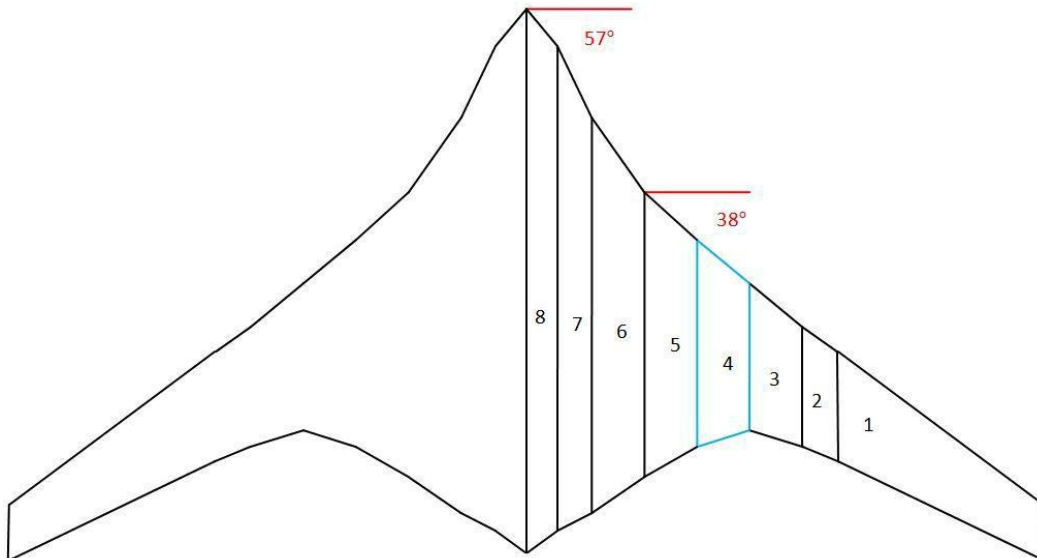


Figure 6.1: Top-down view of BWB design.

(6.1)

Table 6.1: Chord lengths and section areas for BWB

<b>Half-span Chord Lengths and Section Areas</b>				
<b>Section</b>	<b>a (ft)</b>	<b>b (ft)</b>	<b>h (ft)</b>	<b>A (ft<sup>2</sup>)</b>
1	12.82	25.18	48.16	915.10
2	25.18	27.47	8.42	221.58
3	27.47	33.88	12.62	387.28
4	33.88	47.62	12.62	514.44
5	47.62	65.48	12.62	713.86
6	65.48	91.12	12.62	988.42
7	91.12	111.72	7.95	806.13
8	111.72	125.00	7.48	885.45
<b>Total</b>	--	--	<b>122.5</b>	<b>5432.25</b>

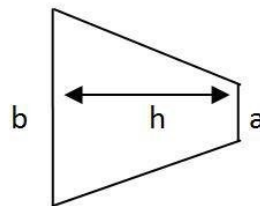


Figure 6.2: Example trapezoid to outline a, b, and h for BWB outline

From figure 6.1, it can be seen that the cockpit protrudes from the body at a steeper angle to allow pilots a greater range of view. The outboard wing sweep of the BWB is 38 degrees, similar to the wing sweep of a B747 [13]. From table 6.1, it can be seen that the centerbody length is 125ft with wingspan of 245ft. The wing tip cord is 12.82ft to allow for greater internal room for fuel tanks and a significantly larger winglet root. The outboard wing taper ratio from section 4 to section 1 is 0.38, similar to other long range jet transports [25].

## 6.2 Passenger Area

The passenger area of the BWB is sectioned into six cabins in a double deck orientation to ease the pressurization process. The seating arrangement is in a three class system in which the major differences between each class are the seat sizes and number of passengers per row. Aisle widths were assumed to be constant and class independent. In designing the lower floor of the passenger area, it was discovered that the outer cabins would not be full sized as a result of the sloping underbelly. By removing the outer two seats and sectioning off the cabin at the isle

end, it was possible to increase the seat width and add extra room for additional luggage or fuel cooling systems. With a 17% airfoil thickness and 125ft centerbody length, the maximum internal height is 21.25ft. This allows for two 7ft tall cabins, a 5ft tall luggage compartment, and 2ft for fuselage and cabin structures. The current design suffers from a lack of capacity in the luggage bay, especially after the landing gear installation. The underbelly of the aircraft may be redesigned in the future for greater luggage capacity, but that would require significant alterations to the outline design. Figure 6.3 illustrates the proposed passenger and luggage areas for the BWB design.

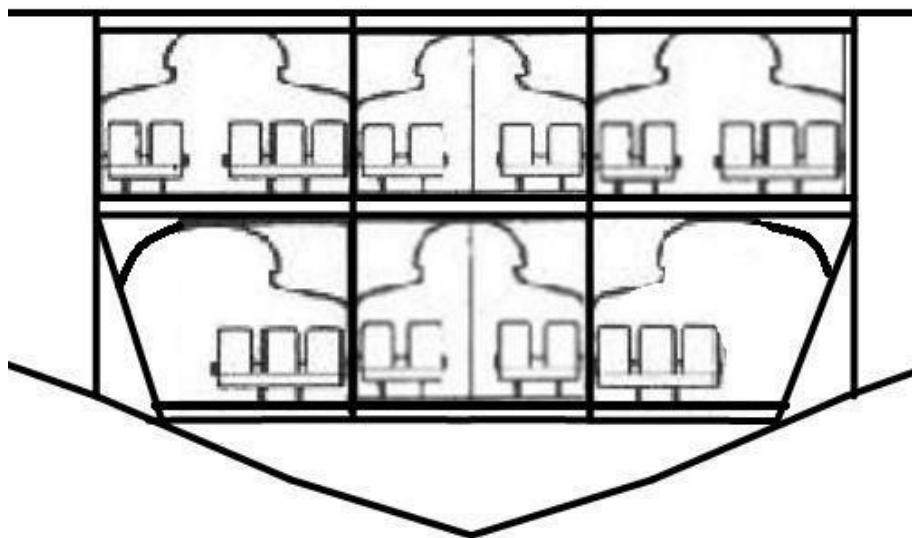


**Figure 6.3: Cross Section of BWB passenger area.**

The two center cabins are closest to the aircraft's roll axis and expected to experience the least amount of motion during roll maneuvers and perturbations. These two cabins will be designated for 1<sup>st</sup> class and have a maximum of 4 seats per row with the largest seats (24in wide). The two lower cabins that were reduced in size allowed for a reduction in the number of people per row and installation of slightly larger seats (22in wide). These two cabins will be designated as 2<sup>nd</sup> class. The remaining upper two cabins have highest passenger density at 5 seats per row and the lowest width seats (20in wide). These two cabins are designated as 3<sup>rd</sup> class. Table 6.2 lists the seating widths per class, number of aisles/seats per cross-section, and total widths of each passenger deck. Seat, aisle, and structural depth widths were selected after reviewing Roskam's fuselage layouts [25].

Table 6.2: Cabin seating and width breakdown.

Component	Individual Width (ft)	Count Upper (# of Seats/Aisles)	Count Lower (# of seats/Aisles)	Width Total Upper (ft)	Width Total Lower (ft)
Aisle	1.67	3	3	5	5
First Class Seat	2.00	4	4	8	8
Second Class Seat	1.83	0	6	0	11
Third Class Seat	1.67	10	0	16.67	0
<b>Overall</b>	--	<b>17</b>	<b>13</b>	<b>29.67</b>	<b>24.00</b>

From table 6.1, the allocated width for sections 7 and 8 is 30.86ft. From table 11, the highest width deck is 29.67ft. The difference between the two widths, 1.19ft, is reserved for cabin wall structures. The outer cabin walls which separate the passenger section from the fuel section should be sufficiently thick, 0.4ft (5in), to protect passengers from possible safety hazards inherent in hydrogen. This leaves each cabin wall to be around 0.167ft (2in) thick.

From table 6.2, the number of passengers per cross section totals 30. Considering the target capacity of 550 passengers, the number of rows needed in the passenger area is calculated to be 18.33, which should be rounded up to 19 rows. Since BWB and flying wing centerbody airfoils typically lose their required thickness around 65% chord length, it is assumed that the total passenger area only takes up around 50% of the total centerbody length, calculated to be 62.5ft. The remaining 15% will be used for the cockpit, crew accommodations, and in-flight supplies. From these constraints, each row is allocated 3.28ft of length. This should be sufficient for seating and leg-room with extra space to be used for in-flight facilities. The calculation for the lengthwise room is given in equation 6.2.

$$\frac{29.67 - 2(0.167)}{1.67} = \frac{29.336}{1.67} = 17.566$$

(6.2)

### 6.3 Hydrogen Fuel Storage

Arguably the most challenging aspect of a hydrogen aircraft is allocating enough space inside the aircraft for its excessive fuel demands. Sections 6 through 1 will be used almost exclusively for fuel storage. However, there are several restrictions on the amount of space used for fuel in these sections. These restrictions allow for enough space to be allocated for structure, fuel lines, coolant systems, and control surface servos.

Noted in section 1.2.1, hydrogen fuel in aircraft should be stored in a series of cylindrical fuel tanks. The equation for the volume of a cylinder is given in equation 18 with cylinder radius,  $r$ , and cylinder height,  $H$ . It should be noted that the fuel tank walls are 0.5in thick for insulation purposes. All fuel tanks sizes and specifications are given in Appendix A. Actual cylinder radius and height is given in the appendix tables. Each section of fuel tanks reserve at least 0.4ft to be used for wing structure, cooling systems, and tank separation. Table 6.3 lists each section's chord restriction and fuel volume.

(18)

**Table 6.3: Fuel Capacity per Section**

Section	Chord Used %	Total Fuel Volume	
		ft <sup>3</sup>	US Gallons
1	50	298.30	2231.43
2	60	144.14	1078.22
3	60	383.25	2866.87
4	70	1454.84	10882.98
5	80	3639.01	27221.64
6	90	7809.84	58421.69
<b>Half-Span Total</b>	--	<b>13729.37</b>	<b>102702.80</b>
<b>Full Length Total</b>	--	<b>27458.74</b>	<b>205405.70</b>

Conservative weight calculations estimated that the fuel requirement would fill 203,575 US gallons. With the current BWB design, it is proven possible to balance hydrogen fuel storage and passenger area. Further research into hydrogen fuel consumption and storage mediums is expected to improve the passenger capacity aboard BWB-LH<sub>2</sub> designs.

### **6.3.1 Hydrogen Fuel Tank Design**

There are two main challenges that fuel tank engineers have to face when designing storage for liquid hydrogen fuel: pressurization and cooling. In cars and planes, liquid hydrogen storage tanks tend to be cylindrical as to pressurize the fuel and alleviate the requirements of a given cooling system. Considering that liquid hydrogen requires a temperature of  $-253^{\circ}$  Celsius to maintain liquid form at 1 atm, pressurizing the fuel tank would greatly reduce that temperature to around  $-100^{\circ}$  Celsius, which is a manageable figure for cooling systems to maintain hydrogen in liquid form [26]. For the BWB-LH<sub>2</sub>, the selected fuel tanks will be a series of cylindrical fuel tanks with a sufficient wall thickness as to strengthen for pressurization. However, the fabrication of such large hydrogen tanks is a significant engineering dilemma which eventually caused the postponement of the X-33 project [27].

The X-33 is a reusable launch vehicle which utilizes a liquid oxygen and liquid hydrogen propellant. The liquid hydrogen fuel tanks were constructed out of carbon fiber reinforced plastics (CFRP), but ultimately failed after microcracks appeared due to the shrinking in the material caused by the cryogenic temperatures of the liquid hydrogen fuel [27]. Since then, materials engineers have researched possible permeability resistant films to coat the composite walls as to prevent such separation in the fuel tank walls. Currently, the most promising fuel tank design is a lightweight interleaved composite for the tank walls of the tank with an inner layer of aluminized Mylar film. The aluminized Mylar film shows substantial resistance to permeability of liquid hydrogen and is able to withstand over 1000 cycles before replacement [27].

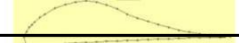
## **7. WING DESIGN**

### **7.1 Centerbody Airfoil**

Centerbody airfoil selection is largely dependent on minimizing the moment coefficient. Unlike the outboard wing, the centerbody should be able to correct negative pitching moments without the use of a horizontal stabilizer. To achieve a low moment coefficient, centerbody airfoils tend to be reflexed towards the trailing edge. From section 6.2, the double deck design of the interior demands a substantially thick airfoil, on the order of 17%. This thickness will need to extend as far down the chord as possible to accommodate the passenger area requirements. To do this, several airfoils were reviewed and altered to include a reflex and push the maximum

thickness location towards the trailing edge. Javafoil v2.23 was utilized to redesign four selected airfoils. After placing the airfoil coordinates into the “Geometry” tab, the next step would be to smooth the surface using tools in the “Modify” tab. After the initial airfoil has been prepared, the redesign can begin in the “Design” tab by modifying the pressure coefficient and iterating the design until the current and target coefficients match. Then the airfoil is once again smoothed in the “Modify” tab and then analyzed in the subsequent tabs for flow, lift, drag, and moment. This process is iterated several times to optimize the redesigned airfoils. Table 7.1 lists four potential centerbody airfoils and their specifications prior to their redesign.

**Table 3: Potential Centerbody Airfoils.**

<b>Airfoil</b>	<b>MS 0317</b>	<b>TsAGI B</b>	<b>L1003</b>	<b>NACA 28117</b>
				
<b>Thickness (%)</b>	17.00	17.17	17.70	16.89
<b>Max thickness</b>				
<b>Chord (%)</b>	37.50	35.76	30.00	28.24
<b>Camber (%)</b>	1.70	2.85	6.50	1.55
<b>Maximum <math>C_L</math></b>	1.75	1.56	1.30	1.65
<b>Max Lift AoA</b>				
<b>(deg)</b>	20.00	15.00	11.00	10.00
<b>Max L/D</b>	80.40	147.27	86.67	143.60
<b>Lift at Max L/D</b>	0.61	1.08	1.30	1.23
<b>AoA at Max L/D</b>	1.75	8.00	11.00	9.00

Although the Liebeck L1003 has the largest thickness, redesign was not well received in the Javafoil program and was left out of consideration. The NACA 28117 airfoil underwent significant transformations from its original shape. The final design performs much like the TsAGI B airfoil. The TsAGI B, being the only double reflex airfoil in the group, was fairly easy to work with, but the airfoil was reluctant to minimize. The MS 0317 airfoil was selected for its low moment coefficient values. The redesigned NACA 28117 and TsAGI B airfoils are located in Appendix B. The redesigned MS 0317 design and moment graph are given in figure 7.1. The moment coefficient dips negative at 6 degrees angle of attack, but the subsequent moments are fairly low in magnitude and should be controllable. The lift to angle of attack plot is given in figure 7.2.

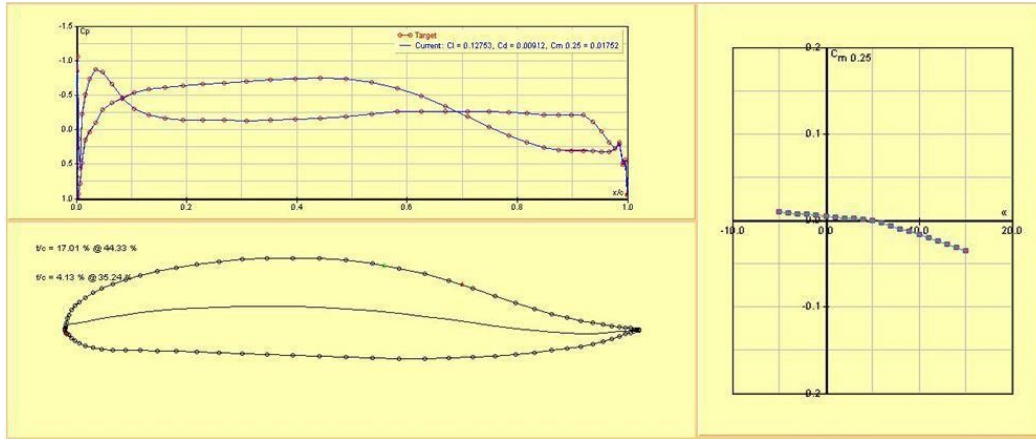


Figure 7.1: MS 0317 Redesigned Airfoil pressure distribution and  $C_m$  vs  $\alpha$

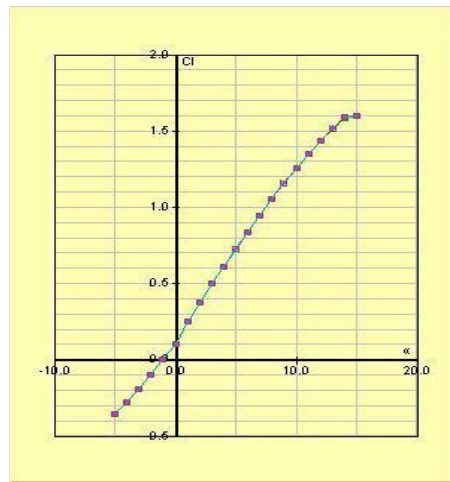


Figure 7.2: MS 0317  $C_l$  versus  $\alpha$

## 7.2 Outboard Airfoil

Outboard airfoil selection is dependent on meeting the expected lift requirements while minimizing the moment coefficient. Symmetrical airfoils at small angles of attack should be able to achieve the required lift for minimal impact on moment coefficient. The NACA 0012 supercritical airfoil is selected for the outboard airfoil as it fulfills all roles adequately. Figure 7.3 provides a coordinate system of the airfoil. Figures 7.4 and 7.5 presents lift and moment diagrams as a function of angle of attack, respectively.

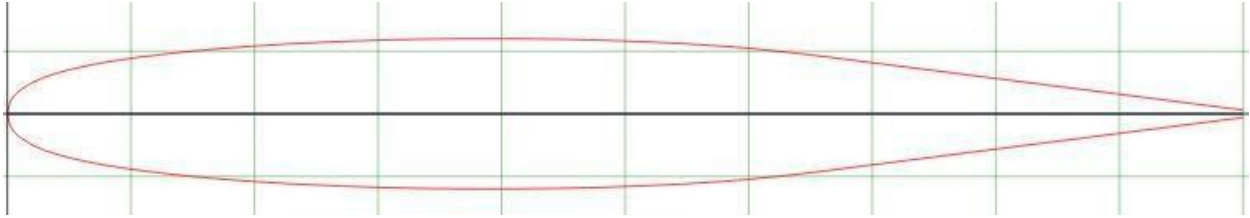


Figure 7.3: NACA 0012 Supercritical Airfoil Outline

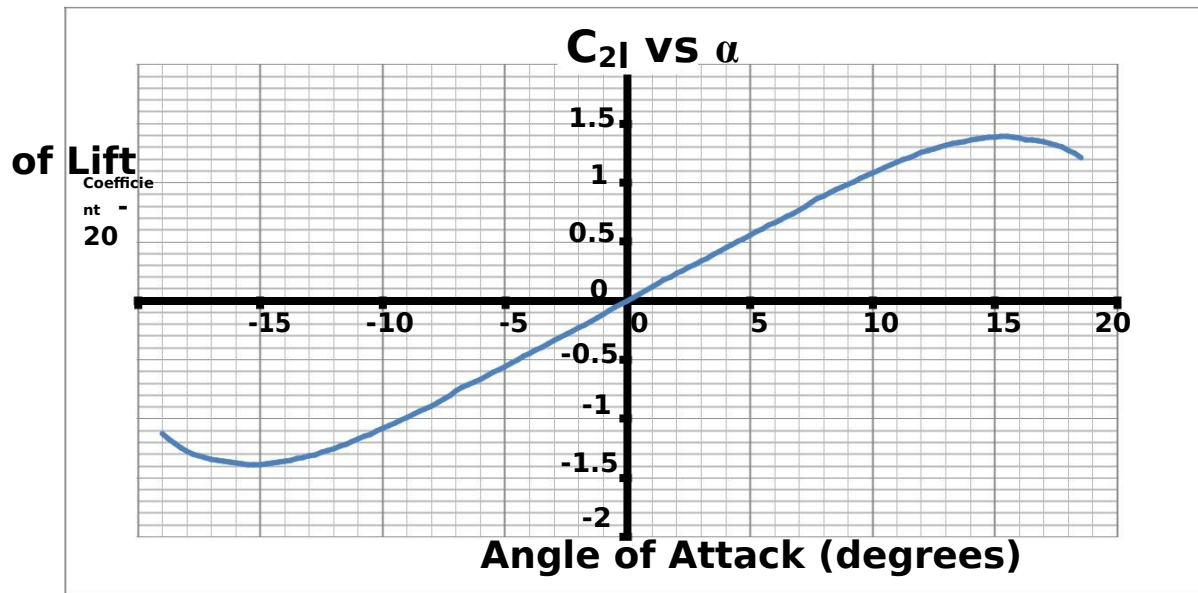


Figure 7.4: Lift and Moment as a function angle of attack for NACA 0012 (SC)

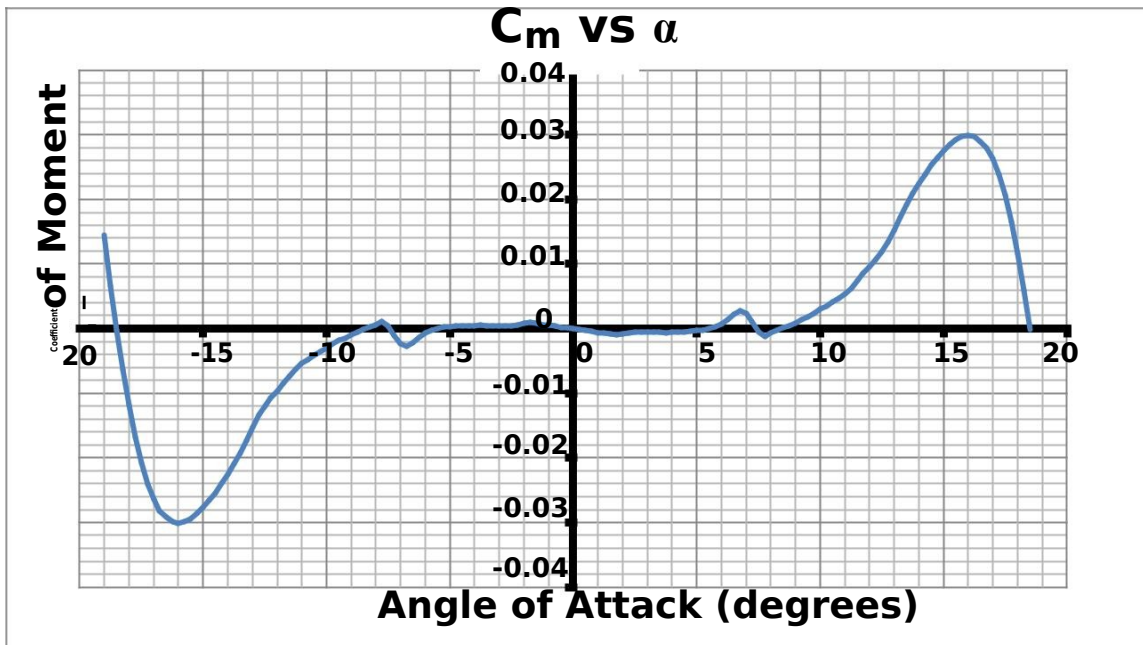


Figure 7.5: Moment as a function of angle of attack for NACA 0012 (SC)

### 7.3 Wing Analysis Program

Experimentation with the “Wing Analysis Program” from [aero.stanford.edu](http://aero.stanford.edu) was able to provide initial values for lift, induced drag, moment, and Oswald efficiency for various angles of attack. After some trial and error, the BWB-LH<sub>2</sub>'s 2D shape was modeled in the program. Altering the incidence values allowed for optimization of the aircraft's wing and centerbody. The initial experimentation results for cruise conditions are given in figure 7.6. Calculating for lift, equation 7.1, with the assumption of steady flight at cruise, resulted in a necessary lift coefficient of 0.238, which matches the program's estimates.

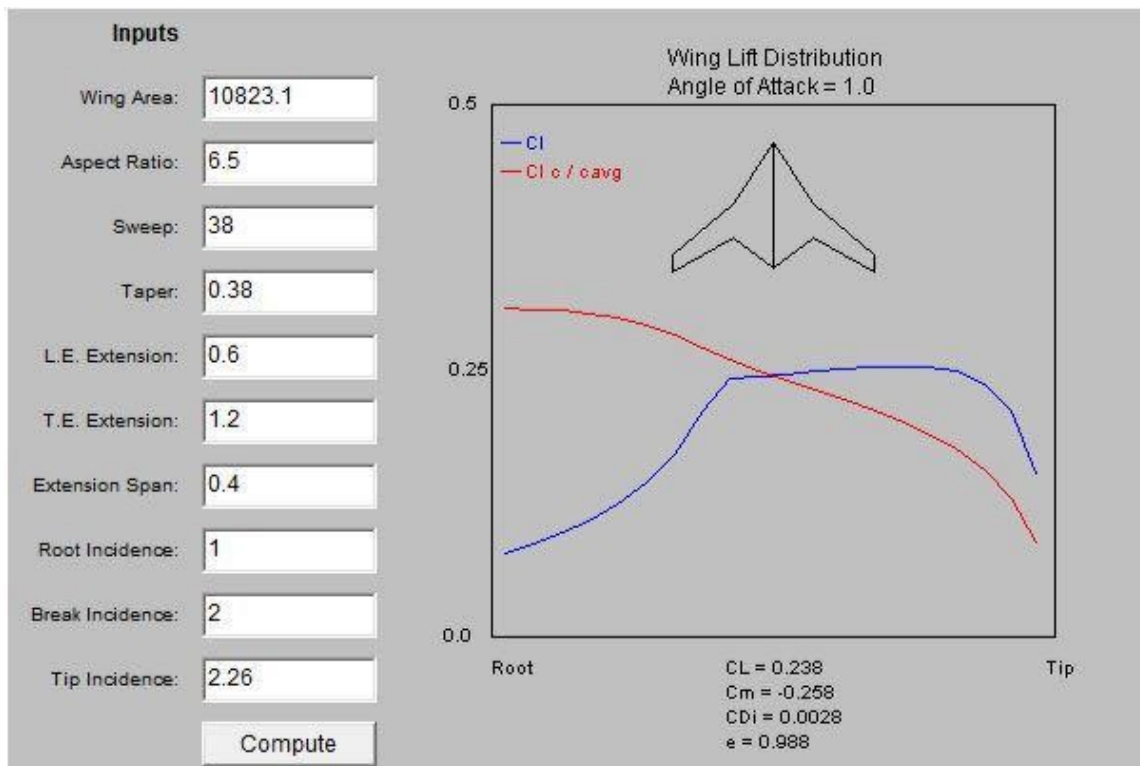


Figure 7.6: Wing Analysis Program Experimentation

(7.1)

## 7.4 Winglet Design

Winglets are installed on the aircraft to impede the formation of wingtip vortices which cause induced drag. Although simply a side effect, the installation of winglets may be able to aid in lateral control as they will be the sole vertical stabilizers on the aircraft. Weirman and Jacob provides a baseline geometry for winglets which can be placed into PECOS to determine the effects of geometry on the L/D and wing bending moments. Figure 7.7 provides an image of their baseline [28].

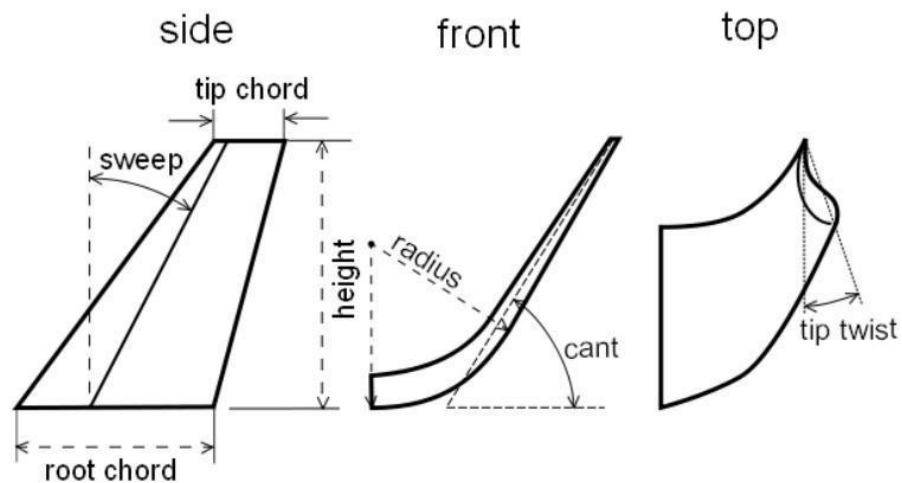


Figure 7.7: Winglet geometry baseline [28]

For the BWB-LH<sub>2</sub>, the tip chord will be a length of 0.3 the root chord length. The root chord length is 12.82ft from table 6.1. The height will be equal to the root chord. The cant angle will be 80 degrees from the horizontal and the twist angle is 0. The airfoil for the winglet will be the NACA 0012 (SC). The vertical stabilizer volume coefficient ( $C_{VT}$ ) is given in equation 7.2. Estimation of length to center of gravity ( $L_{VT}$ ) for the BWB-LH<sub>2</sub> is 50.38ft. Using equation 6.1, surface area of the vertical stabilizer ( $S_{VT}$ ) is calculated to be 214ft<sup>2</sup>. The wingspan ( $b_w$ ) and wing area ( $S_w$ ) are taken from previous sections of the report. The calculated  $C_{VT}$  is 0.004, which is much lower than the recommended 0.09 [22]. This means the lateral control for yaw would be dominated by control methods such as differential thrust or drag.

(7.2)

## 8. LANDING GEAR DESIGN

The multi-bogey landing gear configuration is utilized in the BWB-LH<sub>2</sub>. The multi-bogey design is fairly common in aircraft with gross weights exceeding 400,000 lbs [22, 29]. In previous work, it was expected that the passenger, cockpit, and crew stations would only take up around 65% of the centerbody length. The remaining 35% of the centerbody interior will be used for main landing gear bays and propulsion systems. The underbody area directly beneath the cockpit and crew sections will be used for the nose gear. The nose gear will be a single strut with a dual tire setup that will serve to steer the BWB-LH<sub>2</sub> in taxi. The outermost main gears in the aft are single strut with a six tire setups. The centermost aft gear will be a single strut with a four tire setup. This brings the total of tires to 18, which allows for average tire loads of around 36,100 lbs, well within the range of type VII tires common in jet transports [22]. The position and height of the landing gears are determined based on limitations regarding lateral and longitudinal ground clearance of 5 and 15 degrees respectively [22, 29]. The lateral ground clearance from the landing gear to the wingtip is expected to be well above the recommended 5 degrees. Conservative calculations, considering 8.5ft tall gears placed underneath section 6 from figure 10, place the lateral ground clearance angle at 10 degrees. The longitudinal ground clearance, with 8.5ft tall gears situated at 75% centerbody length is expected to reach the 15 degrees. However, the BWB-LH<sub>2</sub> should install an angle of attack limiter to prevent any tail-strike possibilities. The aft-main gears, placed at 75% centerbody length is well aft of the expected center of gravity. The initial center of gravity is estimated assuming a 3% static margin with the aerodynamic center. With an aerodynamic center at 812in from the nose, the expected center of gravity is around 788in from the nose. The aft landing gears, placed at around 1100in from the nose are well within acceptable range. Figure 8.1 illustrates the proposed layout for the BWB-LH<sub>2</sub> landing gear.

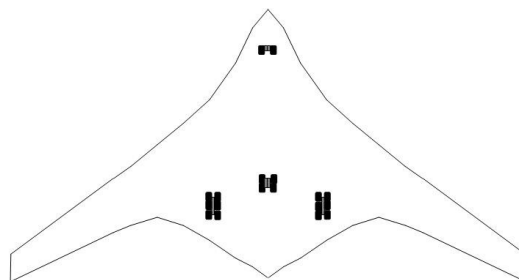


Figure 8.1: Landing Gear Orientation

## 9. WEIGHT AND BALANCE

### 9.1 Fuselage Weight

The weight fraction calculations for fuselage weight detailed in Roskam and Raymer's design texts are not applicable to sizing a BWB's centerbody weight. Fortunately, Kevin R. Bradley's BWB structural analysis provides equations for conceptual centerbody weight sizing. The calculations split fuselage into two different sections: cabin and aft. The main cabin is made up of passenger, crew, pilot, and luggage compartments. The aft section is made up of the landing gear, engine, and fuel systems [30].

The equation for cabin weight is given in equation 9.1 [30]. The term TOGW is the take-off gross weight which is taken from table 8 in the weight summary. The term  $S_{\text{cabin}}$  is the cabin surface area which was assumed to be the fore surface area (0-65% centerbody length). After the calculation, 10% of the weight was deducted for weight savings from using advanced composites [22].

(9.1)

The equation for the aft body weight is given in equation 9.2 [30]. The term  $N_{\text{eng}}$  is the number of engines installed. The term  $S_{\text{aft}}$  is the aft body surface area (66-100% centerbody length). The term  $AR_{\text{aft}}$  is aft taper ratio, calculated to be around 0.5. Similar to the cabin weight, a 10% weight deduction is taken due to advanced composite weight savings [22].

(9.2)

### 9.2 Wing Weight

Although the BWB "melds" the centerbody and the wing, the wing weight can be calculated using Raymer's conceptual weight sizing method. The equation for wing weight is taken from Raymer's cargo and transport aircraft sizing calculations and displayed in equation 9.3 [22]. The term  $N_z$  is the aircraft's ultimate load factor. The terms  $S_w$ ,  $AR$ , and  $AR_{\text{aft}}$  are the

wing's surface area, aspect ratio, and taper ratio, respectively. The term  $(t/c)_{\text{root}}$  is the airfoil's thickness divided by chord length at the root of the wing.

–

(9.3)

### 9.3 Engine Weight

The current BWB-LH<sub>2</sub> design features three GEnx-1B turbofan engines. These engines, originally installed on the Boeing 787, collectively produce a sufficient amount of thrust for the given mission specifications. The equations for calculate nacelle weight is given in equation 9.4 [22]. The term  $K_{\text{ng}}$  is a weight fraction constant for the pylon mounted nacelle. The terms  $N_{\text{Lt}}$ ,  $N_{\text{w}}$ , and  $S_{\text{n}}$  are the nacelle length, width, and wetted area which are calculated using slightly larger dimensions than the actual engine. The dimensions and engine weight,  $W_{\text{ec}}$ , are available from a GEnx-1B data sheet provided by the European Aviation Safety Agency [31]. The weight of the engine controls are calculated using equation 9.5. The term  $L_{\text{ec}}$  is the length from the engine front to the cockpit.

(9.4)

(9.5)

### 9.4 Landing Gear Weight

The landing gears, detailed in section 8, are split up into two categories: nose and main. The equations for nose and main gears are given in equations 9.6 and 9.7, respectively [22]. The terms  $K_{\text{np}}$  and  $K_{\text{mp}}$  are weight fractions for the use of kneeling gears, which the BWB excludes (assume a value of 1). The terms  $L_{\text{n}}$  and  $L_{\text{m}}$  are the lengths for the nose and main gears. The term  $W_{\text{l}}$  is the landing weight, which is assumed to be the BWB-LH<sub>2</sub> with a full payload and no fuel. The term  $N_{\text{l}}$  is the ultimate landing load factor. The term  $N_{\text{mss}}$  is the number of main gear shock struts, assumed to be equal to the number of struts. The stall velocity,  $V_{\text{stall}}$ , is assumed to be 125kts.

(9.6)

(9.7)

## 9.5 Subsystem Weight

The subsystem group consists of a variety of different processes and elements which are crucial to the aircraft's performance. Although several of these categories make up less than 1% of the aircraft's total weight, their positions on the aircraft are important to balancing the center of gravity. The equation for calculating flight controls, equation 9.8, is presented in Roskam's Airplane Design text as the Torenbeek Method. The term  $K_{fc}$  is a weight fraction constant for power controls [32].

–

(9.8)

Included inside the same compartment as flight controls are the instruments. The equation for calculating instrument weight is given in equation 9.9 [22]. The terms  $K_r$  and  $K_{tp}$  are weight fraction constants for reciprocating and turboprop engines, respectively. The term  $N_c$  indicates the number of crew members. The term  $L_f$  represents the fuselage length. The term  $B_w$  represents the wing span.

(9.9)

The equation for electrical subsystem weight is given in equation 9.10 [22]. The equation takes into consideration the system electrical rating,  $R_{kva}$ , electrical routing distance,  $L_a$ , and the number of generators,  $N_{gen}$ . The electrical routing distance is assumed to equal the distance from the cockpit to the aft body and then from the aft body to the wingtips.

(9.10)

The equations for calculating the avionics, air conditioner, and anti-ice system weights are given in equations 9.11, 9.12, and 9.13, respectively [22]. The term  $W_{uav}$  is the weight of the uninstalled avionics, which is assumed to be 1400 lbs. The term  $N_p$  is the number of personnel onboard.

(9.11)

—

(9.12)

(9.13)

The installed APU and hydraulics weights are given in equations 9.14 and 9.15 respectively [22]. The term  $N_f$  is the number of functions performed by controls. The uninstalled APU weight was assumed to be around 700 lbs.

(9.14)

(9.15)

The most difficult system to model, the liquid hydrogen fuel system, was calculated using Raymer's weight sizing method [22]. The term  $V_t$  is the total fuel volume for the aircraft given in weight sizing to be around 203,000 US gallons. The only tanks used on the BWB-LH<sub>2</sub> are self-sealing as hydrogen must not be allowed to leak and turn into a gaseous state. Thus the volume of the integral tanks,  $V_i$  is 0, whereas the self-sealing tank volume,  $V_p$ , contains all 203,000 US gallons of fuel. The term  $N_t$  is the number of tanks onboard. The entire fuel system weight was then increased by 50% to include a cooling system and overall heavier fuel tank build.

— —  
(9.16)

Although there are several individual components inside the cabin area, a general equation for the furnishings weight is given in equation 9.17 [22]. The term  $W_c$  represents the payload weight given in the weight sizing section. The term  $S_f$  is the fuselage wetted area.

(9.17)

## 9.6 Center of Gravity Calculations

The weights for each component excluding payload and fuel are calculated using the Matlab code given in Appendix C. The payload and fuel weights are given in the weight sizing section. The center of gravity was calculated using equation 9.18. The resulting calculations are displayed in table 9.1. The center of gravity travel versus the aircraft weight is plotted in figure 9.1.

—————  
(9.18)

**Table 9.1: Weight Sizing and Center of Gravity Results**

Group	Component	Wi (lbs)	Xi (in)	Wi*xi (in-lbs)
Fuselage	Cabin Weight	66100.00	544.2	35971620.00
	Aft Body	19139.00	1201.5	22995508.50
Wing	Left Wing	45076.00	762	34347912.00
	Right Wing	45076.00	762	34347912.00
Engine	3xGENx 1B+Nacelle	85934.46	1284	110339846.6
	Engine Controls	315.00	76.5	24097.50
Landing Gears	Nose Gear	3147.40	114	358803.60
	Main Gear	30632.00	1116	34185312.00
Equipment/Subsystem	Flight Controls+Instruments	5692.28	76.5	435459.29
	Electrical System	1084.60	240	260304.00
	Avionics	2141.40	51.9	111138.66
	A/C+Anti-Ice	5664.70	360	2039292.00
	APU	1540.00	1080	1663200.00
	Furnishing	63544.00	465	29547960.00
	Hydraulics	340.70	948	322984.93
	Fuel System	27986.00	720	20149920.00
Payload/Fuel	Passengers	96250.00	712.5	68578125.00
	Luggage	22450.00	762	17106900.00
	Mid Cabin Crew	875.00	712.5	623437.50
	Aft Cabin Crew	875.00	975	853125.00
	Forward Cabin Crew	875.00	228	199500.00
	Trapped Fuel and Oil	3246.00	741.12	2405675.52
	Liquid Hydrogen Fuel	120284.00	741.12	89144878.08
Summary		W (lbs)	--	X <sub>cg</sub> (in)
	No Payload, Full Fuel	526943.54	--	794.49
	No Payload, No Fuel (W <sub>E</sub> )	403413.54	--	810.83
	Maximum Payload, No Fuel	524738.54	--	789.85
	Maximum Payload Full Fuel (W <sub>TO</sub> )	648268.54	--	780.56

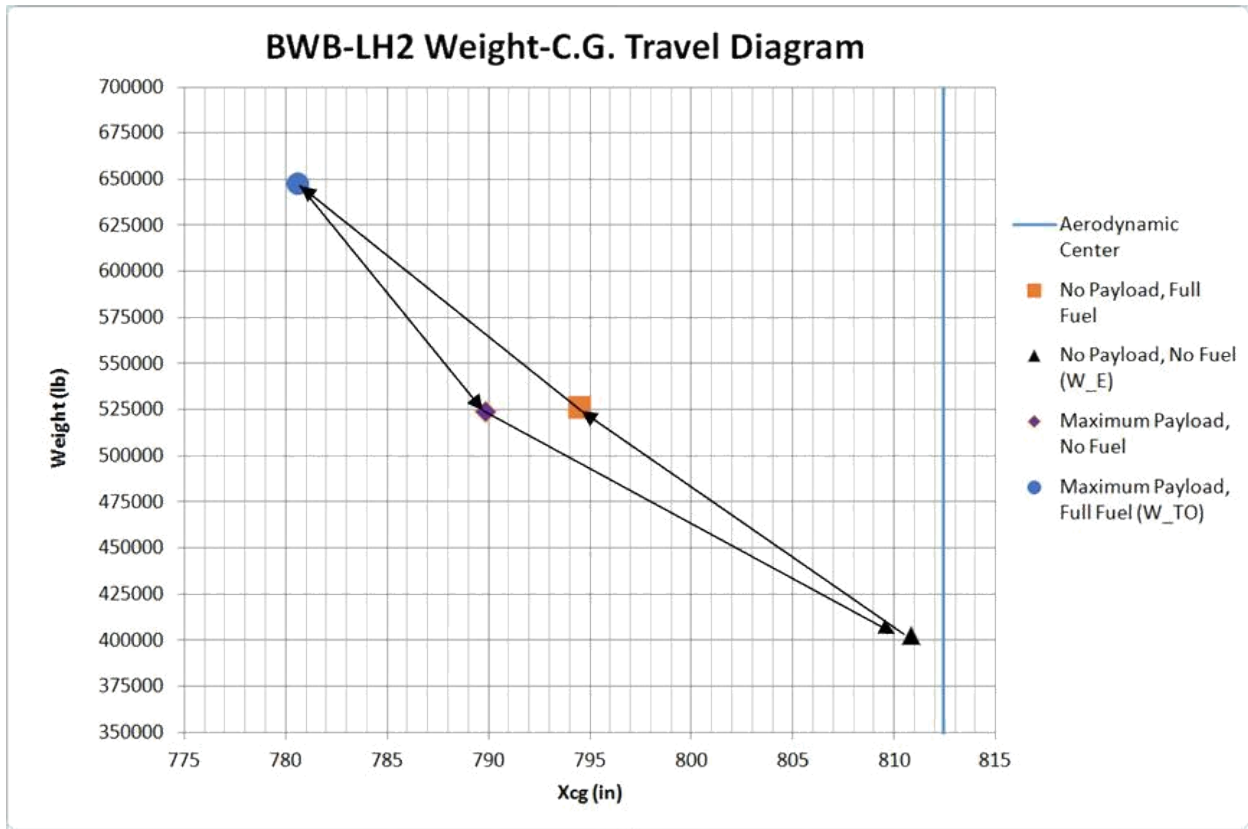


Figure 9.1: Center of Gravity Travel Diagram as it relates to aircraft weight.

From figure 9.1, it is evident that all flight scenarios were able to restrict the center of gravity from moving aft of the aerodynamic center. This was done through careful positioning of the landing gears and main engines. The center of gravity travel between  $W_E$  and  $W_{TO}$  is roughly 30 inches with a maximum static margin of 3.8% from the aerodynamic center. It should be noted that hydrogen's weight properties have a substantial effect on the center of gravity travel. Changing the fuel from hydrogen to kerosene will cause the fully fueled aircraft to be excessively nose heavy.

## 10. STABILITY ANALYSIS

### 10.1 Longitudinal Stability

Longitudinal stability analysis of a blended wing body is a critical step in the development process. If the static stability of the aircraft is neutral or negative or the aircraft exceeds its centerbody airfoil performance values, then the aircraft will experience the

“tumbling” phenomenon. The tailless nature of flying wings and blended wing bodies may simplify several of the coefficient calculations, but complicates the overall analysis process [33]. The longitudinal state space system is given in equation 10.1. The output matrix (C) is an identity matrix of length equal to A and feedthrough matrix (D) is a zero matrix. The state matrix (A) and input matrix (B) for axial velocity(u), angle of attack( $\alpha$ ), pitch rate(q), and pitch angle( $\theta$ ) are given in equation 10.2 [34]. A Matlab code for performing open loop longitudinal analysis is given in Appendix D.

$$\begin{aligned}
 & \hspace{10em} (10.1) \\
 A = & \begin{matrix} \text{-----} & \text{-----} & \text{-----} & \text{-----} \\ & \text{-----} & \text{-----} & \text{-----} \\ & & \text{-----} & \text{-----} \\ & & & \text{-----} \end{matrix} \\
 B = & \begin{matrix} \text{-----} \\ \text{-----} \end{matrix} \\
 & \hspace{10em} (10.2)
 \end{aligned}$$

While it was initially intended to provide an accurate stability analysis of the BWB-LH<sub>2</sub> in cruise flight conditions, several assumptions inevitably led to results which were unsuitable for the report. However, regardless of the results, BWB designs will almost certainly require controllers and limiters to control oscillations from perturbations and to prevent tumbling.

### 10.1.1 Important Parameters

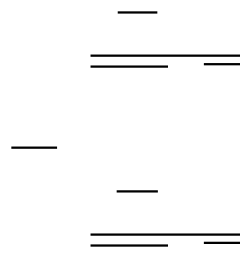
One of the most important coefficient changes between conventional and tailless aircraft is pitch stiffness ( $C_{m\alpha}$ ). As a result of a reflexed centerbody airfoil in place of a horizontal stabilizer,  $C_{m\alpha}$  simplifies to a relation between static margin ( $K_n$ ) and lift curve slope ( $a_w$ ). Here static margin is simply the difference between non-dimension distances of the center of gravity and the aerodynamic center with respect to mean aerodynamic chord. For most blended wing bodies, the average  $K_n$  values tend to be between 0.02 and 0.08. The equation for  $C_{m\alpha}$  for general aircraft and its tailless simplification is given in equation 10.3[33].

$$\text{---} \quad \text{---} \quad (10.3)$$

This simplification of  $C_{m\alpha}$  limits the static margin to positive values, meaning that the center of gravity can never travel aft of the aerodynamic center or the aircraft would cause susceptibility to the tumbling phenomenon. For the current BWB-LH<sub>2</sub> design, the calculated  $C_{m\alpha}$  term is -0.16 radians per second, which is very small due to the low static margin value. Further iterations to the weight analysis section should provide greater separation between the center of gravity and the aerodynamic center.

A notable coefficient change as a result of the tailless configuration is pitch damping ( $C_{mq}$ ). Without a proper horizontal stabilizer, the  $C_{mq}$  value is expected to be fairly small. In the open loop system, oscillations would take an extremely long time to dampen out [33]. A final notable coefficient to pay attention to is the elevator control power ( $C_{m\delta_e}$ ). Since the moment arm in tailless aircraft between the elevator and the center of gravity is much shorter than a conventional aircraft, the control surfaces must have a greater deflection, larger surface area, or a combination of the two. This leads coefficients such as change in drag due to elevator deflection ( $C_{D\delta_e}$ ) and change in lift due to elevator deflection ( $C_{L\delta_e}$ ) to be non-negligible values [33].





(10.6)

There are disadvantages to this method. The first disadvantage is that it isn't very applicable to the current engine setup. All three engines are setup around 85% of the chord length, and oriented very close to the centerline of the centerbody. For the method to work, the engines will need to be repositioned to the ends of the centerbody to prevent large differences in throttling during yaw control. The second disadvantage is that there would be no yaw control in the event that an outer engine fails. A combination with alternative yawing method would allow for minor changes to the current engine configuration and give each method a backup in the event of failure.

### 10.2.2 Split Aileron/Deceleron Method

The second method for controlling yaw moment is by using split ailerons or decelerons at the wingtips to produce a differential drag force. As these control surfaces open up, depicted in figure 10.1, they separate the flow and produce a certain amount of pressure drag which is dependent on their total deflection,  $\delta$  [36].

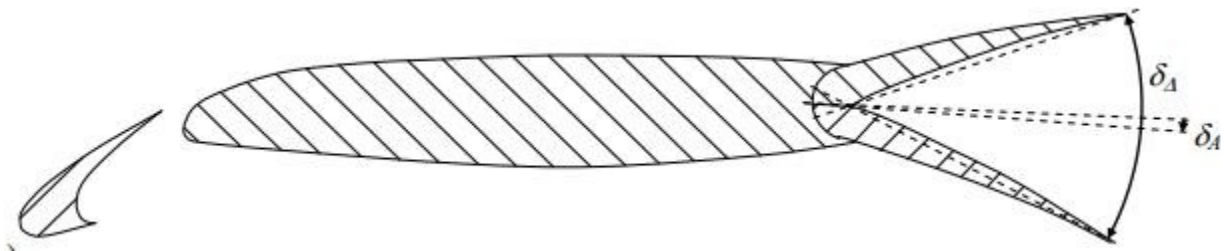


Figure 10.1: Slatted airfoil featuring a deceleron control surface [4].

Calculation of coefficients for lateral stability is expected to be similar to the coefficients in the thrust differential method with  $y_e$  being the distance between the decelerons to the center of gravity. The  $\delta$  value should be placed into a function to calculate the drag force of the plates

as a function of the degrees of deflection. Such calculations can be performed using CFD or methods outlined in Hoerner's *Fluid Dynamic Drag* textbook [37].

Deflection of this control surface would inadvertently cause a change in the lift of the deflected wing. Aileron input from a controller would be necessary to correct the adverse roll effects. The obvious downside to this method is the large amounts of drag it produces, thus decreasing the overall efficiency of the aircraft. In combination with thrust differential method, the deflection of this control surface would be minimized.

## 11. DRAG POLAR

### 11.1 Drag Polar Plots

After several estimations, the final wetted area for the aircraft is expected to be around  $26750\text{ft}^2$  which correlates into a lower zero-lift drag. Figure 11.1 illustrates the drag versus lift for the several configurations outlined in section 4.3. Figure 11.2 illustrates the clean configuration L/D confirmation, which is estimated to reach a maximum of about 23. Although these numbers sound promising, the study was a simple class-1, and would need to be revisited before the final design. Appendix F provides the code for generating these two drag polar analyses.

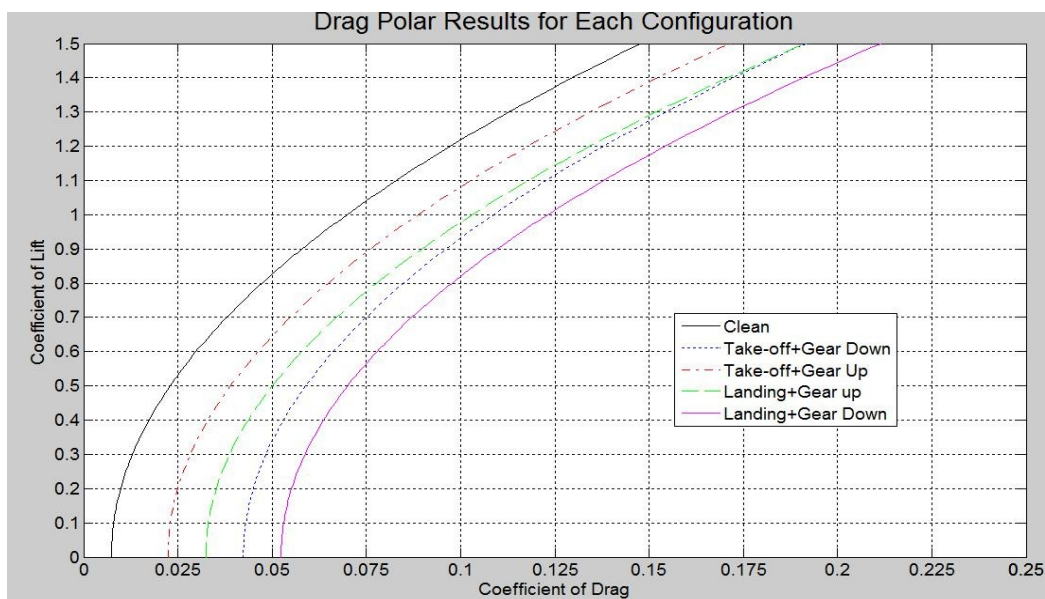
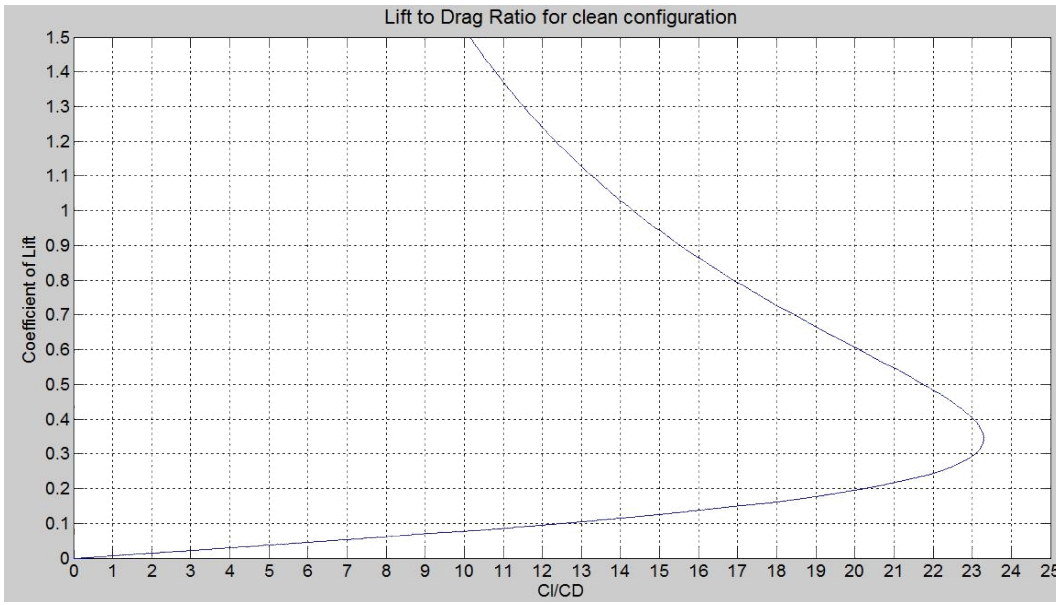


Figure 11.1: Drag Polar for each phase configuration



**Figure 11.2: Lift to drag ratio for clean configuration**

## 11. DISCUSSION

Future work regarding the BWB-LH<sub>2</sub> should focus on optimizing the individual sections and components outlined in the report. From the very first stages of this report, several of the calculated components were taken to be fairly conservative. Research into hydrogen fuel consumption in jet engines and their respective efficiencies will allow for higher accuracy in fuel volume estimations. Design of aircraft applicable liquid hydrogen fuel tanks should yield proper fuel tank design specifications including dimensions and weights. With the combination of accurate fuel volume and tank design, the safety spacing between tanks and the other internal compartments is expected to grow. The centerbody airfoil design was complicated due to nature of relatively high airfoil thickness. The ideal centerbody airfoil would be able to maintain a positive moment coefficient at significantly higher angles of attack. Further iterations of the MS-0317 airfoil and CFD simulations of the finished centerbody would yield better performance than this report's centerbody design. Further analysis on landing gear design should provide sample tire selection and an explanation of which runway surfaces are allowable for the aircraft.

A major factor in the design of the BWB-LH<sub>2</sub> relies heavily on the validity of the class-2 weight analysis presented in this report. The static margin between the center of gravity and aerodynamic center is exceedingly small, thus requiring a detailed class-3 weight analysis before any prototype can be constructed. With the aid of CAD programs (ie. SolidWorks), modeling of

the BWB-LH<sub>2</sub> with all components and their weights appropriately installed would provide higher accuracy information on weight and moment of inertia calculations. In addition to a more accurate weight analysis model, further exploration into the aircraft's component materials may yield a significantly lighter aircraft. Since hydrogen burns at a much lower temperature than Jet-A1, the materials in the thrust chamber of the GEnx-1B turbofan may be transitioned into a lighter material as a result of a lower heat resistance requirement. Composite fuel tanks with a film to ward against permeability of liquid hydrogen would also aid in the BWB-LH<sub>2</sub> weight reduction. Adjustment of these components in the modeling program may allow for a larger static margin, and thus a more positively stable aircraft. Further examination into the open loop stability matrices for both longitudinal and lateral cases should provide control engineers with a basis to design controllers which will limit the oscillations following a perturbation.

In terms of feasibility, the BWB-LH<sub>2</sub> design is able to meet all performance goals adequately, although the actual mission of comfortable transport of passengers is hindered by the design trade-offs to accommodate liquid hydrogen fuel. The weaknesses of the current design relate majorly to the internal compartment design, including the absence of passenger windows, thin walls, and the difficulty in installing escape/exit hatches. Aside from future work into this specific commercial aircraft, it would be interesting to re-design the BWB-LH<sub>2</sub> to accommodate cargo instead, thus reducing several of the design constraints in place to comfortably seat passengers.

## 12. CONCLUSION

This report has proven that liquid hydrogen is a viable alternative to current kerosene based jet fuels when paired with the unconventional BWB design configuration. The merger of liquid hydrogen fuel into a BWB design has proven to mitigate each other's respective faults such as the low energy density of hydrogen and the low maximum lift coefficient of BWB. The switch away from Jet-A1 to liquid hydrogen is expected to reduce aviation pollution by a significant amount. When paired with the fact that the supply of liquid hydrogen is closely related with the availability of hydrogen carrying molecules (ie. H<sub>2</sub>O), the supply of liquid hydrogen is seemingly limitless. While the price of Jet-A1 isn't expected to equate to the price of liquid hydrogen until the year 2040, aviation companies should start examining alternative designs and fuels to prevent a rapid rise in flight operation costs.

## REFERENCES

1. Federal Aviation Administration. "Aviation Emissions, Impacts & Mitigation: A Primer". Office of Environment and Energy. January 2015.
2. Seeckt, K. and Scholz, D. "Jet Versus Prop, Hydrogen Versus Kerosene For a Regional Freighter Aircraft". Deutscher Luft- und Raumfahrtkongress 121195. 2009.
3. Koroneos, C.J. and Moussiopoulos N. "Cryoplane-Hydrogen vs. Kerosene as Aircraft Fuel". 7th International Conference on Environmental Science and Technology. September 2001.
4. Peifeng, L., Binqian Z., Yingchun C., Changsheng Y., and Yu, L. *Aerodynamic Design Methodology for Blended Wing Body Transport*. Chinese Journal of Aeronautics Vol. 25. 2012.
5. van Zon, Nout. "Liquid Hydrogen Powered Commercial Aircraft: Analysis of technical feasibility of sustainable liquid hydrogen powered commercial aircraft in 2040". Technical University of Delft.
6. Langston, L.S. "As the Turbine Turns". Global Gas Turbine News. December 2013.
7. Guynn, M.D., Freeh, J.E. and Olson, E.D. "Evaluation of a Hydrogen Fuel Cell Powered Blended-Wing-Body Aircraft Concept for Reduced Noise and Emissions". NASA 212989. February 2004.
8. Verstraete, D. "On the Energy Efficiency of Hydrogen-Fuelled Transport Aircraft". International Journal of Energy Vol. 40. 2015.
9. Dehpanah, P. and Nejat, A. "The Aerodynamic Design Evaluation of a Blended-Wing-Body Configuration". Aerospace Science and Technology Vol. 43. 2015.
10. Ordoukhanian, E. and Madni, A.M. "Blended Wing Body Architecting and Design: Current Status and Future Prospects". Conference on Systems Engineering Research. 2014.
11. NASA Facts. "The Blended-Wing-Body". Langley Research Center. 1997.
12. Liebeck, R.H. "Design of a Blended Wing Body Subsonic Transport". Journal of Aircraft Vol. 41, No. 1, January-February 2004.
13. "747-8 Airplane Characteristics for Airport Planning" Available Online: [http://www.boeing.com/assets/pdf/commercial/airports/acaps/747\\_8.pdf](http://www.boeing.com/assets/pdf/commercial/airports/acaps/747_8.pdf)
14. "777X Technical Specs". URL: <http://www.boeing.com/commercial/777x/> [Cited 25 September 2015].

15. "Introducing the new GE9X Turbofan Engine". URL:  
<http://www.ge.com/stories/aviation-ge9x> [Cited 25 September 2015].
16. "A380 Specifications". URL:  
<http://www.airbus.com/aircraftfamilies/passengeraircraft/a380family/specifications/>  
[Cited 25 September 2015].
17. "A340-600 Specifications". URL:  
<http://www.airbus.com/aircraftfamilies/passengeraircraft/a340family/a340-600/specifications/> [Cited 25 September 2015].
18. Roskam, J. "Airplane Design Part I: Preliminary Sizing of Airplanes." Lawrence KS: DARCorp 2003.
19. Matson, D. "Design of a Medium Range Blended Wing Body Transport." Graduate Research Project, Department of Mechanical and Aerospace Engineering, San Jose State University, CA, 2007.
20. Woodridge, E.T. "History of the Flying Wing: The Nortrop Bombers," Century of Flight. Available online: <http://www.century-of-flight.net/Aviation%20history/flying%20wings/Northrop%20bombers.htm>
21. "B-2 Spirit Fact Sheet" Available online:  
<http://www.af.mil/AboutUs/FactSheets/Display/tabid/224/Article/104482/b-2-spirit.aspx>
22. Raymer, D.P. "Aircraft Design: A Conceptual Approach." Washington D.C.: AIAA 1992.
23. GE Aviation "GE's GENx-2B Engine for the New Boeing 747-8 Airplane Achieves 70,000 lbs. Takeoff Thrust in First Test". March 12, 2008. Available online:  
[http://www.geaviation.com/press/genx/genx\\_20080312.html](http://www.geaviation.com/press/genx/genx_20080312.html)
24. Buch Jr., G.M. "AMC's Future Strategic Airlifter: The Blended Wing Body?" Graduate Research Project. Department of Operational Sciences, Air Force Institute of Technology, OH, 2010.
25. Roskam, J. "Airplane Design Part II: Preliminary Configuration Design and Integration of the Propulsion System." Lawrence KS: DARCorp 2003
26. Zalosh, R., "CNG and Hydrogen Vehicle Fuel Tank Failure Incidents, Testing, and Preventative Measures," *2008 AIChE Spring National Meeting*, AIChE, New Orleans, LA, 2008.
27. Grimsley, B.W., Cano, R.J., Johnston, N.J., Loos, A.C., and McMahon, W.M., "Hybrid Composites for LH2 Fuel Tank Structure," NASA Langley Research Center, Hampton, VA, Jan. 2001.

28. Weierman, J., and Jacob, J.D., "Winglet Design and Optimization for UAVs," 28<sup>th</sup> AIAA Applied Aerodynamics Conference, June 28 – July 1, 2010, Chicago, IL, United States, 2010
29. Roskam, J. "Airplane Design Part IV: Layout, Design of Landing Gear and Systems." Lawrence KS: DARCorp 2003
30. Bradley, K.R. "A Sizing Methodology for the Conceptual Design of Blended-Wing-Body Transports," NASA/CR-2004-213016
31. "Type Certificate Data Sheet: GENx-1B, GENx-2B". URL: [http://easa.europa.eu/system/files/dfu/EASA-TCDS-E.102\\_\(IM\)\\_General\\_Electric\\_Company\\_GENx\\_Series\\_engines-05-24062013.pdf](http://easa.europa.eu/system/files/dfu/EASA-TCDS-E.102_(IM)_General_Electric_Company_GENx_Series_engines-05-24062013.pdf) [Cited 2 February 2016].
32. Roskam, J. "Airplane Design Part V: Component Weight Estimation." Lawrence KS: DARCorp 2003
33. Rahman, N. "Propulsion and Flight Controls Integration for the Blended Wing Body Aircraft" Ph. D. Thesis, Department of Aerospace Sciences School of Engineering, Cranfield University, Cranfield, England. 2009.
34. Roskam, J. "Airplane Flight Dynamics and Automatic Flight Controls Pt. 1" Lawrence KS:DARCorp 2001.
35. Lu, L. "Utilization of Differential Thrust for Lateral/Directional Stability of a Commercial Aircraft with a Damaged Vertical Stabilizer" (2015).*Master's Theses*. Paper 4649.
36. Jung, U. S., "Alternative Air Brake Concepts for Transport Aircraft Steep Approach", München: Dr. Hut, 2012.
37. Hoerner, S. F., "Fluid-Dynamic Drag," Hoerner Fluid Dynamics, 1965.

## Appendix A-Individual Fuel Tank Sizes

Table A.1: Section 1 Fuel Tank Sizes

Section 1					
Column	r (ft)	H (ft)	r <sub>actual</sub> (ft)	H <sub>actual</sub> (ft)	Volume (ft <sup>3</sup> )
1	0.5	6.41	0.458333	6.326667	4.1753
2	0.5	6.541489	0.458333	6.458156	4.262077
3	0.5	6.672979	0.458333	6.589645	4.348854
4	0.5	6.804468	0.458333	6.721135	4.435631
5	0.5	6.935957	0.458333	6.852624	4.522407
6	0.5	7.067447	0.458333	6.984113	4.609184
7	0.5	7.198936	0.458333	7.115603	4.695961
8	0.5	7.330426	0.458333	7.247092	4.782738
9	0.5	7.461915	0.458333	7.378582	4.869514
10	0.5	7.593404	0.458333	7.510071	4.956291
11	0.5	7.724894	0.458333	7.64156	5.043068
12	0.5	7.856383	0.458333	7.77305	5.129845
13	0.5	7.987872	0.458333	7.904539	5.216621
14	0.5	8.119362	0.458333	8.036028	5.303398
15	0.5	8.250851	0.458333	8.167518	5.390175
16	0.5	8.38234	0.458333	8.299007	5.476952
17	0.5	8.51383	0.458333	8.430496	5.563728
18	0.5	8.645319	0.458333	8.561986	5.650505
19	0.5	8.776809	0.458333	8.693475	5.737282
20	0.5	8.908298	0.458333	8.824965	5.824058
21	0.5	9.039787	0.458333	8.956454	5.910835
22	0.5	9.171277	0.458333	9.087943	5.997612
23	0.5	9.302766	0.458333	9.219433	6.084389
24	0.5	9.434255	0.458333	9.350922	6.171165
25	0.5	9.565745	0.458333	9.482411	6.257942
26	0.5	9.697234	0.458333	9.613901	6.344719
27	0.5	9.828723	0.458333	9.74539	6.431496
28	0.5	9.960213	0.458333	9.876879	6.518272
29	0.5	10.0917	0.458333	10.00837	6.605049
30	0.5	10.22319	0.458333	10.13986	6.691826
31	0.5	10.35468	0.458333	10.27135	6.778603
32	0.5	10.48617	0.458333	10.40284	6.865379
33	0.5	10.61766	0.458333	10.53433	6.952156
34	0.5	10.74915	0.458333	10.66582	7.038933
35	0.5	10.88064	0.458333	10.7973	7.12571
36	0.5	11.01213	0.458333	10.92879	7.212486

37	0.5	11.14362	0.458333	11.06028	7.299263
38	0.5	11.27511	0.458333	11.19177	7.38604
39	0.5	11.4066	0.458333	11.32326	7.472817
40	0.5	11.53809	0.458333	11.45475	7.559593
41	0.5	11.66957	0.458333	11.58624	7.64637
42	0.5	11.80106	0.458333	11.71773	7.733147
43	0.5	11.93255	0.458333	11.84922	7.819924
44	0.5	12.06404	0.458333	11.98071	7.9067
45	0.5	12.19553	0.458333	12.1122	7.993477
46	0.5	12.32702	0.458333	12.24369	8.080254
47	0.5	12.45851	0.458333	12.37518	8.167031
48	0.5	12.59	0.458333	12.50667	8.253807

Table 4: Section 2 Fuel Tank Sizes

Section 2					
Column	r (ft)	H (ft)	r_actual (ft)	H_actual (ft)	Volume (ft <sup>3</sup> )
1	1.25	16.482	1.208333	16.39867	75.21976
2	1.25	15.108	1.208333	15.02467	68.9173

Table A.3: Section 3 Fuel Tank Sizes

Section 3					
Column	r (ft)	H (ft)	r_actual (ft)	H_actual (ft)	Volume (ft <sup>3</sup> )
1	1.75	20.328	1.708333	20.24467	185.6119
2	1.5	18.405	1.458333	18.32167	122.4133
3	1.25	16.482	1.208333	16.39867	75.21976

Table A.4: Section 4 Fuel Tank Sizes

Section 4						
Row	Column	r (ft)	H (ft)	r_actual (ft)	H_actual (ft)	Volume (ft <sup>3</sup> )
1	1	2	33.334	1.958333 3	33.25067	400.6115
	2	2	28.525	1.958333 3	28.44167	342.6716
	3	1.75	23.716	1.708333 3	23.63267	216.6745
2	1	1.75	33.334	1.708333 3	33.25067	304.8565
	2	1.5	28.525	1.458333 3	28.44167	190.0284



Table A.5: Section 5 Fuel Tank Sizes

Section 5						
Row	Column	r (ft)	H (ft)	r_actual (ft)	H_actual (ft)	Volume (ft <sup>3</sup> )
1	1	2	55.658	1.958333	55.57467	669.5761
	2	2	48.0675	1.958333	47.98417	578.1241
	3	2	40.477	1.958333	40.39367	486.672
2	1	2	55.658	1.958333	55.57467	669.5761
	2	2	48.0675	1.958333	47.98417	578.1241
	3	1.75	40.477	1.708333	40.39367	370.3466
3	1	1.25	55.658	1.208333	55.57467	254.9179
	2	0.5	48.0675	0.458333	47.98417	31.66728

Table A.6: Section 6 Fuel Tank Sizes

Section 6						
Row	Column	r (ft)	H (ft)	r_actual (ft)	H_actual (ft)	Volume (ft <sup>3</sup> )
1	1	2	82.008	1.958333	81.92467	987.0469
	2	2	70.47	1.958333	70.38667	848.0345
	3	2	58.932	1.958333	58.84867	709.022
2	1	2	82.008	1.958333	81.92467	987.0469
	2	2	70.47	1.958333	70.38667	848.0345
	3	2	58.932	1.958333	58.84867	709.022
3	1	2	82.008	1.958333	81.92467	987.0469
	2	2	70.47	1.958333	70.38667	848.0345
	3	1.3	58.932	1.258333	58.84867	292.7372
4	1	1.5	82.008	1.458333	81.92467	547.3664
	2	0.5	70.47	0.458333	70.38667	46.45187



## Appendix B – Redesigned Airfoils

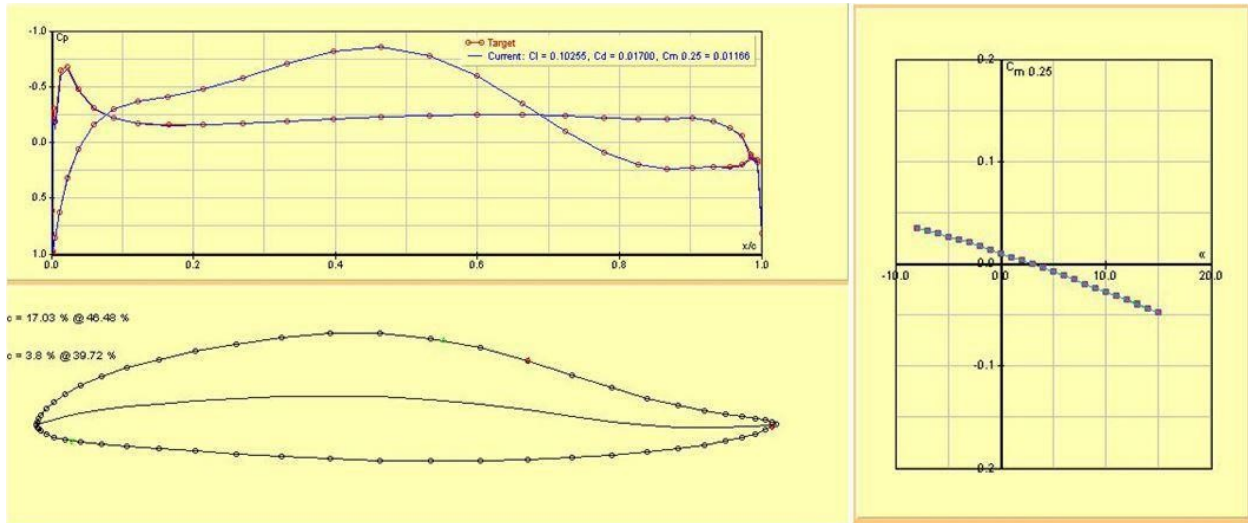


Figure B.1: TsAGI B -17% Airfoil Retool Design and Cm data

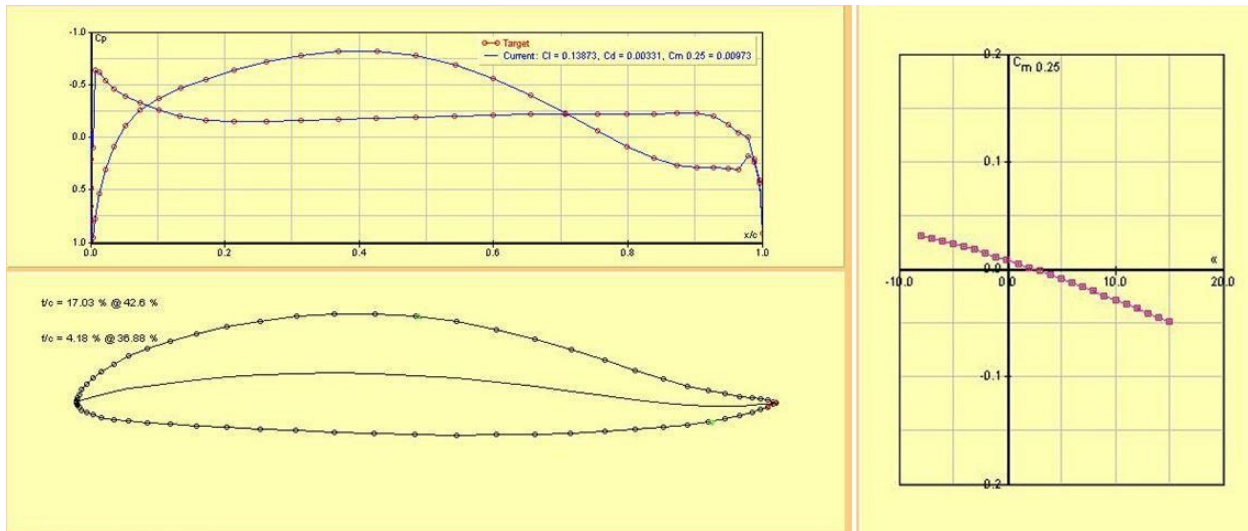


Figure B.2: NACA 28117 Retool Design and Cm data

## Appendix C – Weight Sizing Code

```
% Component Weight Calculations for the BWB-LH 2 Aircraft Design % Matthew Smith
% San Jose State University Aerospace Department % AE295B Masters Aerospace
Project
% Created 2/10/2016 % Edited 2/27/2016 clear
all;

close all; clc ;
% Variables descriptions/equations taken from: % Raymer, Aircraft Design, p 405-
407;
% Roskam, Airplane Design Part V: Component Weight Estimation, p 98-99 % Bradley, A Sizing Methodology for the Conceptual
Design of
% Blended-Wing-Body Transports A=6; %Aspect Ratio B_w=245; %Wing
Span, ft

K_fc = 0.64; %Torenbeek Method constant for power controls K_mp=1.0; %1.126 for kneeling gear; = 1.0
otherwise K_np=1.017; %1.017 for pylon-mounted nacelle; = 1.0 otherwise K_np=1.0; %1.15 for kneeling
gear; = 1.0 otherwise
K_r=1.0; %1.133 if reciprocating engine; = 1.0 otherwise; K_tp=0.793; %0.793 if turboprop; = 1.
0 otherwise
L_a=425; %electrical routing distance, generators to avionics to cockpit, ft L_ec=125*3; %length from engine front to cockpit-total if multiengine, ft
L_f=125; %total fuselage length

L_m=102; %length of main landing gear, in L_n=102; %nose gear length, in N_c=15;
%number of crew

N_eng=3; %number of engines
N_f=5; %number of functions performed by controls (typically 4-7) N_gen=3; %number of generators (typically = Neng)
N_g=4.4; %ultimate landing load factor = Ngear x 1.5 N_L=15.4; %nacelle length, ft (Assume = Engine length) GE
Genx-1B. N_m=2; %number of mechanical functions (typically 0-2) N_mw=16; %number of main wheels
N_mss=3; %number of main gear shock struts N_nw=2; %number of nose
wheels
N_t=50; %number of fuel tanks, equation meant for kerosene, higher tank number for LH2 calculations N_w=17; %nacelle width, ft
R_kva=50; %system electrical rating, kv . A (typically 40-60 for transports,110-160 for fighters & bombers) S_aft=2400; %Aft body surface area, ft
S_cs=1000; %total area of control surfaces, ft2. Assume ~9% of total surface area S_f= S_aft+S_cabin*2.5; %fuselage wetted area, ft2
S_w=10823; %trapezoidal wing area, ft2 taper_aft=0.5; %Aft taper
taper_wing=0.38; %Wing taper tc_root=17.01; %Root t/c TOGW=649384;
%Take-Off Gross Weight, lbs
```



## Appendix D – Longitudinal Stability Code (Open Loop)

```
% Longitudinal Stability
% Aircraft characteristics
S=10865; %Wing Area ft^2
cbar=60; %Chord Length,
ft b=245; %Wing Span ft
Xcg=.52;
W=648269; %Weight lbf
g=32.17; %Gravity in ft/s^2
m=W/g; %Mass in lbm
rho=0.0237; %Density
lb/ft^3 M=0.85; %Mach
L=cbar; %Length of centerbody chord, ft
%Conditions: Cruise
U1=827; %True Airspeed in ft/s
qbar=0.5*rho*U1^2; %Dynamic Pressure in lb/ft^2
alpha=1; %Angle of attack, 1 degree in cruise
gamma=0; %Assume 0 deg degree flight path angle
theta=alpha+gamma; %Steady State
%Moment of inertias in slug*ft^2
R_barx=0.32; %R_bar is a nondimensional radii of gyration for flying
wing R_bary=0.32;
R_barz=0.51;
Ix=(b^2*W*R_barx^2)/(4*g);
Iy=(L^2*W*R_bary^2)/(4*g);
Iz=((b+L)/2)^2*W*R_barz^2/(4*g);
Ixz=0;
%Thrust Stability Coefficients
C_Tx1=; %Trim x-thrust coefficient
C_Txu=; %Change in x-thrust with velocity (Assume 0)
%Lift Stability Coefficients
C_L1=; %Trim Lift Coefficient
C_Lu=M^2/(1-M^2)*C_L1; %Change in lift coefficient due to velocity
C_L0=; %Initial lift
C_Lalpha=; %Change in lift with angle of attack
C_Lalphadot=; %Downwash lag lift
C_Lq=; %Lift due to pitching
C_Ld_elev=; %Change in lift due to
elevator %Drag Stability Coefficients
C_D1=; %Trim drag coefficient
C_Du=; %Change in drag as a result of velocity (Assume 0, max M=0.85)
C_D0=; %Zero Lift Drag
C_Dalpha=; %Change in drag due to angle of attack
C_Dd_elev=; %Change in drag due to elevator deflection (Assume negligible)
%Moment Stability Coefficients
C_M1=; %Trim Pitch Coefficient
C_MT1=; %Trim Thrust pitch moment coefficient
C_Mu=; %Change in moment due to velocity (Assume negligible due to constant Xcg
and Xac)
C_Malpha=; %Change in moment due to angle of
attack C_Malphadot=; %Downwash lag moment
C_Mq=; %Change in moment due to pitching
C_MTu=; %Change in moment due to thrust (assume negligible)
C_MTalpha=; %Change in moment due to thrust angle of attack (assume negligible)
C_Md_elev=; %Change in moment due to elevator deflection
%Dimensional Stabilities
X_u=(-qbar*S*(C_Du+2*C_D1))/(m*U1);
X_Tu=(qbar*S*(C_Txu+2*C_Tx1))/(m*U1);
X_Alpha=(-qbar*S*(C_Dalpha-C_L1))/m;
X_d_elev=(-qbar*S*C_Dd_elev)/m; Z_u=-
qbar*S*(C_Lu+2*C_L1)/(m*U1);
Z_Alpha=-qbar*S*(C_Lalpha+C_D1)/m;
```

```

Z_Alphadot=-qbar*S*cbar*C_Lalphadot/(2*m*U1);
Z_q=-qbar*S*cbar*C_Lq/(2*m*U1);
Z_d_elev=-qbar*S*C_Ld_elev/m;
M_u=qbar*S*cbar*(C_Mu+2*C_M1)/(Iy*U1);
M_Tu=qbar*S*cbar*(C_MTu+2*C_MT1)/(Iy*U1);
M_alpha=qbar*S*cbar*C_Malpha/Iy;
M_Talpha=qbar*S*cbar*C_MTalpha/Iy;
M_q=qbar*S*cbar^2*C_Mq/(2*Iy*U1)
M_Alphadot=qbar*S*cbar^2*C_Malphadot/(2*Iy*U1);
M_d_elev=qbar*S*cbar*C_Md_elev/Iy;
DENOM=U1-Z_Alphadot;
%Matrix Form
A(1,1)= X_u+X_Tu;
A(1,2)= X_Alpha;
A(1,3)= 0;
A(1,4)= -g*cosd(theta);
A(2,1)= Z_u/DENOM;
A(2,2)= Z_Alpha/DENOM;
A(2,3)= (Z_q+U1)/DENOM;
A(2,4)= (-g*sind(theta))/DENOM;
A(3,1)= M_u+M_Tu+((M_Alphadot*Z_Alpha)/DENOM);
A(3,2)= M_alpha+M_Talpha+((M_Alphadot*Z_Alpha)/DENOM);
A(3,3)= M_q+((M_Alphadot*(Z_q+U1))/DENOM);
A(3,4)= (-M_Alphadot*g*sin(theta))/DENOM;
A(4,1)=0;
A(4,2)=0;
A(4,3)=1;
A(4,4)=0;
B(1,1)= X_d_elev;
B(2,1)= Z_d_elev/(DENOM);
B(3,1)= M_d_elev+(M_Alphadot*Z_d_elev)/DENOM;
B(4,1)=0;
%State Space Matrices
A
B
C = eye(length(A))
D = [0;0;0;0]
%State Space
sys = ss(A,B,C,D);
%Simulation for perturbation
SimTime = 60;
t = [0:1e-2:SimTime]'; % simulation time vector
u = zeros(length(t),1); % input vector
indx_t_1 = find(t == 1); % we need to find when the step will kick in
u_stp_in = u; % create step input
u_stp_in(indx_t_1:end,1) = 1*pi/180; % construct step input in
[RAD] [y_ksim_stp, t_ksim_stp] = lsim(sys,u_stp_in,t); figure(1),

subplot(4,1,1), plot(t_ksim_stp, y_ksim_stp(:,1))
title('Axial Velocity Perturbation') xlabel('Time
(sec)'),ylabel('u [ft/sec]'), subplot(4,1,2),
plot(t_ksim_stp, y_ksim_stp(:,2)) title('\alpha
Perturbation')
xlabel('Time (sec)'),ylabel('\alpha [rad/sec]')
subplot(4,1,3), plot(t_ksim_stp, y_ksim_stp(:,3))
xlabel('Time (sec)'),ylabel('q [ft/sec]')
title('Pitch Rate Perturbation')
subplot(4,1,4), plot(t_ksim_stp, y_ksim_stp(:,4))
xlabel('Time (sec)'),ylabel('\theta [rad/sec]')
title('\theta Perturbation')
%Transfer Functions
[num,den] = ss2tf(A,B,C,D);
%Elevator Deflection to axial acceleration

```

```

disp('TF from \delta e --> u')
disp('----- ')
TF_n2u = zpk(tf(num(1,:),den))
%Elevator Deflection to angle of attack
disp('TF from \delta e --> \alpha')
disp('----- ')
TF_n2w = zpk(tf(num(2,:),den))
%Elevator Deflection to pitch rate
disp('TF from \delta e --> q')
disp('-----')
TF_n2q = zpk(tf(num(3,:),den))
%Elevator Deflection to pitch angle
disp('TF from \delta e --> \theta')
disp('-----')
TF_n2theta = zpk(tf(num(4,:),den))
%Storing the eigenvectors and eigenvalues for the longitudinal case
[EigVec, EigVal] = eig(A);
%A routine to pair the Eigenvectors to the eigenvalues
for ii = 1:length(A)
disp(['Eigenvector associated with the ',num2str(ii),'
eigenvalue'])
disp('-----')
EigVal(ii,ii),EigVec(:,ii),
end
%%Damping and Frequency
damp(A)
%
%%Bode Plots
figure(2),
bode(sys(1,1))
title('Bode diagram: \delta e \rightarrow u')
figure(3),
bode(sys(2,1))
title('Bode diagram: \delta e \rightarrow \alpha')
figure(4),
bode(sys(3,1))
title('Bode diagram: \delta e \rightarrow q')
figure(5),
bode(sys(4,1))
title('Bode diagram: \delta e \rightarrow \theta')

```

## Appendix E – Lateral Stability Code (Open Loop)

```
%% Lateral Stability
% Aircraft characteristics
S=10865; %Wing Area ft^2
cbar=90; %Chord Length,
ft b=245; %Wing Span ft
Xcg=.52;
W=648269; %Weight lbf g=32.17;
%Gravity in ft/s^2 m=W/g;
%Mass in lbm rho=0.023697;
%Density lb/ft^3 M=0.85; %Mach
L=125; %Length of centerbody chord,
ft %Conditions: Cruise
U1=827; %True Airspeed in ft/s
qbar=0.5*rho*U1^2; %Dynamic Pressure in lb/ft^2
V_t=U1;
%Moment of inertias in slug*ft^2
R_barx=0.24; %R_bar is a nondimensional radii of gyration for fuselage mounted
engines on jet transports.
R_bary=0.36; R_barz=0.44;
Ix=(b^2*W*R_barx^2)/(4*g);
Iy=(L^2*W*R_bary^2)/(4*g);
Iz=((b+L)/2)^2*W*R_barz^2/(4*g);
Ixz=0;

%Coefficients
C_YBeta=;
C_Yp=; C_Yr=;
C_Yda=;
C_LBeta=;
C_Lp=; C_Lr=;
C_Lda=;
C_NBeta=;
C_Np=; C_Nr=;
C_Nda=;
%Derivatives

Y_v=qbar*S/(V_t)*C_YBeta;
Y_p=qbar*S*b/(V_t)*C_Yp;
Y_r=qbar*S*b/(V_t)*C_Yr;
Y_da=qbar*S*C_Yda;
L_v=qbar*S*b/(V_t)*C_LBeta;
L_p=qbar*S*b^2/(V_t)*C_Lp;
L_r=qbar*S*b^2/(V_t)*C_Lr;
L_da=qbar*S*b*C_Lda;
N_v=qbar*S*b/(V_t)*C_NBeta;
N_p=qbar*S*b^2/(V_t)*C_Np;
N_r=qbar*S*b^2/(V_t)*C_Nr;
N_da=qbar*S*b*C_Nda;
%Matrix Form
A(1,1)= Y_v;
A(1,2)= Y_p+W1;
A(1,3)= (Y_r-U1);
A(1,4)= g*cosd(theta);
A(2,1)= L_v;
A(2,2)= L_p;
A(2,3)= L_r;
A(2,4)= 0;
A(3,1)= N_v;
```

```

A(3,2)= N_p;
A(3,3)= N_r;
A(3,4)= 0;
A(4,1)=0;
A(4,2)=1;
A(4,3)=tand(theta);
A(4,4)=0;
B(1,1)= Y_da;
B(2,1)= L_da;
B(3,1)= N_da;
B(4,1)=0;
A
B
C = eye(length(A))
D = [0;0;0;0]
%State Space
sys = ss(A,B,C,D);
%Simulation for perturbation
SimTime = 60;
t = [0:1e-2:SimTime]'; % simulation time vector
u = zeros(length(t),1); % input vector
indx_t_1 = find(t == 1); % we need to find when the step will kick in
u_stp_in = u; % create step input
u_stp_in(indx_t_1:end,1) = 1*pi/180; % construct step input in
[RAD] [y_ksim_stp, t_ksim_stp] = lsim(sys,u_stp_in,t); figure(1),

subplot(4,1,1), plot(t_ksim_stp, y_ksim_stp(:,1))
title('Side Velocity')
xlabel('Time (sec)'),ylabel('v [ft/sec]'),
subplot(4,1,2), plot(t_ksim_stp, y_ksim_stp(:,2))
title('Roll Rate Perturbation')
xlabel('Time (sec)'),ylabel('p [rad/sec]')
subplot(4,1,3), plot(t_ksim_stp, y_ksim_stp(:,3))
xlabel('Time (sec)'),ylabel('r [ft/sec]')
title('Yaw Rate Perturbation')
subplot(4,1,4), plot(t_ksim_stp, y_ksim_stp(:,4))
xlabel('Time (sec)'),ylabel('\phi [rad/sec]')
title('Roll Angle Perturbation')
%Transfer Functions
[num,den] = ss2tf(A,B,C,D);
%Aileron Deflection to Side Velocity
disp('TF from \delta a --> v')
disp('-----')
TF_n2u = zpk(tf(num(1,:),den))
%Aileron Deflection to Roll Rate
disp('TF from \delta a --> p')
disp('-----')
TF_n2w = zpk(tf(num(2,:),den))
%Aileron Deflection to Yaw Rate
disp('TF from \delta a --> r')
disp('-----')
TF_n2q = zpk(tf(num(3,:),den))
%Aileron Deflection to Roll Angle
disp('TF from \delta a --> \phi')
disp('-----')
TF_n2theta = zpk(tf(num(4,:),den))
%Storing the eigenvectors and eigenvalues for the longitudinal case
[EigVec, EigVal] = eig(A);
%A routine to pair the Eigenvectors to the eigenvalues
for ii = 1:length(A)
disp(['Eigenvector associated with the ',num2str(ii),'
eigenvalue'])
disp('-----')
EigVal(ii,ii),EigVec(:,ii),

```

```
end
% %Damping and Frequency
damp(A)
%
% %Bode Plots
figure(2),
bode(sys(1,1))
title('Bode diagram:  $\delta a \rightarrow v$ ')
figure(3),
bode(sys(2,1))
title('Bode diagram:  $\delta a \rightarrow p$ ')
figure(4),
bode(sys(3,1))
title('Bode diagram:  $\delta a \rightarrow r$ ')
figure(5),
bode(sys(4,1))
title('Bode diagram:  $\delta a \rightarrow \phi$ ')
```

## APPENDIX F- Drag Polar Calculation and Plotting

```
% by: Matthew Smith, Masters student at San Jose State University
% Edited: 5/1/2016
% Purpose: To plot the drag polars of various configurations for a BWB.
clear all;
close all;
clc;
AR=6; %Aspect Ratio
S_wet=26750; %Current wetted area estimate, ft^2
S_ref=10873; %Reference area=wing area for a BWB
C_fe=0.003; %Skin friction coefficient
CD_0_clean=S_wet/S_ref*C_fe; %Zero-Lift Drag Coefficient
dCD_0_to_down=0.035; %Change in Zero-Lift Drag for take-off configuration
with gears down.
dCD_0_to_up=0.015; %Change in Zero-Lift Drag for take-off configuration with
gears up.
dCD_0_landing_down=0.045; %Change in Zero-Lift Drag for landing configuration
with gears down.
dCD_0_landing_up=0.025; %Change in Zero-Lift Drag for landing configuration
with gears up.
e_clean=0.85; %Clean configuration Oswald's efficiency
e_takeoff=0.8; %Take-off configuration Oswald's efficiency
e_landing=0.75; %Landing configuration Oswald's efficiency
CL=[0:0.01:1.5]; %Coefficient of lift CD_clean=CD_0_clean+CL.^2/
(pi()*AR*e_clean); %Clean coefficient of drag
CD_to_down=(CD_0_clean+dCD_0_to_down)+CL.^2/(pi()*AR*e_takeoff); %Take-
off+gear down coefficient of drag
CD_to_up=(CD_0_clean+dCD_0_to_up)+CL.^2/(pi()*AR*e_takeoff); %Take-off+gear up
coefficient of drag CD_landing_up=(CD_0_clean+dCD_0_landing_up)+CL.^2/
(pi()*AR*e_landing); %Landing+gear up coefficient of drag
CD_landing_down=(CD_0_clean+dCD_0_landing_down)+CL.^2/(pi()*AR*e_landing); %La
nding+gear down coefficient of drag

Lift2Drag_clean=CL./CD_clean; %Lift to Drag
%Plot of CL vs CD for each configuration
figure, plot(CD_
clean,CL, 'k', 'LineWidth',1)
hold on
plot(CD_ to_down,CL, 'b:', 'LineWidth',1) hold
on plot(CD_ to_up,CL, 'r-.', 'LineWidth',1)
hold on plot(CD_
landing_up,CL, 'g--', 'LineWidth',1) hold on
plot(CD_landing_down,CL, 'm', 'LineWidth',1)

title('Drag Polar Results for Each Configuration')
legend('Clean', 'Take-off+Gear Down', 'Take-off+Gear Up', 'Landing+Gear
up', 'Landing+Gear Down')
ylabel('Coefficient of Lift')
xlabel('Coefficient of Drag')
figure,
plot(Lift2Drag_clean,CL)
title('Lift to Drag Ratio for clean configuration')
ylabel('Coefficient of Lift')
xlabel('Cl/CD')
```